Calculation of Uncertainty in the (U-Th)/He System

Peter E. Martin[1], James R. Metcalf[1], Rebecca M. Flowers[1]

[1]Department of Geological Sciences, University of Colorado Boulder, CO 80309

Correspondence to: Peter E. Martin (Peter.Martin-2@colorado.edu)

5 **Abstract.** Currently, there is no standardized approach for reporting date uncertainty in the (U-Th)/He system, partly due to the fact that the methods and formulae for calculating single-grain uncertainty have never been fully described and published. This creates challenges for interpreting the expected distribution of dates within individual samples and for comparing dates generated by different labs. Here we publish two procedures to derive (U-Th)/He single-grain date uncertainty (linear and Monte Carlo uncertainty propagation), based on input ^{4}He, radionuclide, and isotope-specific F_T

10 (alpha-ejection correction) values and uncertainties. We also describe a newly released software package, HeCalc, that performs date calculation and uncertainty propagation for (U-Th)/He data. Propagating uncertainties in ^{4}He and radionuclides using a compilation of real (U-Th)/He data (N = 1978 apatites and 1753 zircons) reveals that the uncertainty budget in this dataset is dominated by uncertainty stemming from the radionuclides, yielding median relative uncertainty values of 2.9% for apatite dates and 1.7% for zircon dates (1s equivalent). When uncertainties in F_T of 2% or 5% are

15 assumed and additionally propagated, the median relative uncertainty values increase to 3.5% and 5.8% for apatite dates, and 2.6% and 5.2% for zircon dates. The potentially strong influence of F_T on the uncertainty budget underscores the importance of ongoing efforts to better quantify and routinely propagate F_T uncertainty into (U-Th)/He dates. Skew is generally positive and can be significant, with ~14% of apatite dates and ~5% of zircon dates in the data compilation characterized by skew of 10% or greater. This outcome indicates the value of applying Monte Carlo uncertainty propagation to identify samples with

20 substantially asymmetric uncertainties that should be considered during data interpretation. The formulae published here and the associated HeCalc software can aid in more consistent and rigorous (U-Th)/He uncertainty reporting, which also is a key first step in quantifying whether multiple aliquots from a sample are overdispersed, with dates that differ beyond what is expected from analytical and F_T uncertainties.

1 Introduction

25   Geochronology and thermochronology by the (U-Th)/He method was initially developed as a reliable technique approximately three decades ago (Farley et al., 1996; Wernicke and Lippolt, 1994; Wolf et al., 1996; Zeitler et al., 1987). Since that time, numerous advances such as the ability to measure the (U-Th)/He date of individual grains (e.g., House et al., 2000), improvements in kinetic models to account for the effects of radiation damage accumulation and annealing on He diffusion kinetics (e.g., Flowers et al., 2009; Gautheron et al., 2009; Guenthner et al., 2013), and the development of thermal

30 history modeling tools that improve interpretation of these data (Gallagher, 2012; Ketcham, 2005) have led to the widespread application of this technique and large amounts of data generation. However, with this progress has come recognition of the need to more rigorously and consistently report uncertainties on individual (U-Th)/He dates (Flowers et al., 2022; Ketcham et al., 2022). For example, the intra-sample variability of (U-Th)/He dates often exceeds that predicted by analytical uncertainty, both due to interpretable variation from differences in He diffusion kinetics among grains of the same

35 sample and due to scatter from other factors (e.g., Brown et al., 2013; Fitzgerald et al., 2006; Flowers et al., 2022b). Better accounting for the uncertainties of individual analyses is a key step in determining whether multiple individual analyses from a sample are actually "over-dispersed", and would help develop a more complete understanding of the causes of data dispersion by allowing the scatter attributable to analytical uncertainty to be subtracted from the overall dispersion pattern. In addition, more rigorous uncertainty reporting would improve confidence in large-N datasets, facilitate inter-laboratory data

40 comparisons, and ultimately increase the precision and accuracy of thermal history reconstructions.

One current challenge to comprehensive uncertainty propagation is that, although individual laboratories have derived the methods for propagating uncertainty components into single-grain (U-Th)/He dates, these methods and the resulting formal analytical uncertainty in (U-Th)/He dates have never been described or thoroughly assessed in the literature. It also is unclear if different labs propagate uncertainties in the same manner. Uncertainty propagation in the (U-Th)/He system is complicated by the fact that the age equation has no analytical solution, precluding the direct application of typical uncertainty propagation formulae that combine individual uncertainty components in quadrature through a given function. This problem may be circumvented by approximations of the He age equation that solve directly for time (e.g., Meesters and Dunai, 2005), or by the use of the general "error propagation equation" using the first derivatives of the uncertainty components with respect to time (Bevington and Robinson, 2003). However, linear uncertainty propagation methods rely on an assumption that the derivative of the first term of the Taylor series is a linear function at the scale of the uncertainties being combined (Bevington and Robinson, 2003; McLean et al., 2011). As this assumption is often violated in the (U-Th)/He system, uncertainties have the potential to be skewed (i.e., asymmetric), and uncertainties propagated using standard linear uncertainty propagation may be inaccurate.

Comprehensive uncertainty accounting on individual (U-Th)/He dates involves propagating not only the analytical uncertainties associated with measurements of parent and daughter amounts, but also propagating uncertainties associated with alpha-ejection corrections (FT corrections, which account for He ejected from the crystal via alpha decay). The analytical uncertainty on parent and daughter amounts is generally well-characterized, and the geometric uncertainty on FT values is increasingly well-constrained (e.g., Cooperdock et al., 2019; Glotzbach et al., 2019; Zeigler et al., 2022). As FT uncertainties are better quantified, propagating both analytical and FT uncertainties into the reported uncertainty of (U-Th)/He dates is desirable (e.g., Flowers et al., 2022a).

Here we explain how analytical and F_T uncertainties in (U-Th)/He dates may be combined to derive a single-grain (U-Th)/He date uncertainty. To address the shortcomings of linear uncertainty propagation, we adopt primarily a Monte Carlo approach to quantitatively constrain (U-Th)/He uncertainty. This procedure is both accurate and mathematically simple, and enables evaluation of asymmetric uncertainties (which linear uncertainty propagation does not provide). For completeness and to ease retrospective data comparisons, we also include a method to propagate uncertainty through the calculation of a (U-Th)/He date that relies on more traditional linear uncertainty propagation. In addition, this manuscript presents a new program written in Python 3.8 termed HeCalc (Helium date and uncertainty Calculator; Martin, 2022) that is capable of both Monte Carlo and linear methods of uncertainty propagation. We conclude by using HeCalc to reduce a compilation of real data to determine the typical contributions of each uncertainty component to date uncertainty in actual practice.

2 Background: uncertainty components in (U-Th)/He dates

The currently quantifiable uncertainties on single-grain (U-Th)/He dates include analytical uncertainties associated with parent and daughter isotope measurements and geometric uncertainties associated with alpha-ejection corrections. These are discussed in detail in Flowers et al. (2022a) and summarized more briefly here. We use the word "uncertainty" as a probabilistic statement of the distribution of repeated measurements (e.g., for a ^{238}U measurement of 10 ± 1 µg/g at 1σ, 68.27% of repeated measurements will fall between 9 and 11 µg/g), while "error" refers to the deviation of a measured value from the true value. The uncertainty in decay constants is negligible relative to other sources of uncertainty and results in systematic error across all (U-Th)/He measurements, and therefore is not incorporated in our uncertainty calculation methods.

In the (U-Th)/He technique, the parent nuclides (Uranium, Thorium, and Samarium; ^{238}U, ^{235}U, ^{232}Th, ^{147}Sm) are typically measured using inductively coupled plasma mass spectrometry (ICP-MS), while the daughter product (Helium; ^{4}He) is usually measured on a quadrupole or magnetic sector noble gas mass spectrometer. Most commonly, quantification of ^{4}He and its parent nuclides is performed via isotope dilution to permit conversion from isotopic ratio measurements to molar amounts. Given the measurements of parent and daughter products, a (U-Th)/He date may be calculated using the equation for ^{4}He ingrowth

$$^4\text{He} = 8\,^{238}\text{U}\left(e^{\lambda_{238}t}-1\right) + 7\,^{235}\text{U}\left(e^{\lambda_{235}t}-1\right) + 6\,^{232}\text{Th}\left(e^{\lambda_{232}t}-1\right) + ^{147}\text{Sm}\left(e^{\lambda_{147}t}-1\right)$$

where each nuclide is given as an amount, t is time, and λ is the decay constant for each parent nuclide given in the subscript.

Because of the kinetic energy associated with alpha decay, individual alpha particles (i.e., ^{4}He nuclei) travel
90 between 4 and 34 µm in solid matter before coming to rest, depending on the mineral density and parent or intermediate daughter nuclide (Farley et al., 1996; Ketcham et al., 2011). This redistribution of the daughter product can cause He ejection from a crystal. By assuming a homogenous parent nuclide distribution, measuring the physical dimensions of a single grain, and applying a geometric model to those physical dimensions, the proportion of alpha particles retained in a grain (the fraction trapped; F_T) can be calculated for each nuclide's mean stopping distance (Ketcham et al., 2011). Determination of
95 grain dimensions to calculate F_T is usually accomplished via size measurement of individual grains using photomicrographs with a calibrated digital camera (Cooperdock et al., 2019; Glotzbach et al., 2019). Using the F_T parameter, the effects of alpha ejection on a date can be corrected using a modified version of the ^{4}He ingrowth equation with the isotope-specific F_T values ($^{238}F_T$, $^{235}F_T$, $^{232}F_T$, $^{147}F_T$) included (Ketcham et al., 2011):

$$^4He = 8\,^{238}F_T\,^{238}U\left(e^{\lambda_{238}t}-1\right)+7\,^{235}F_T\,^{235}U\left(e^{\lambda_{235}t}-1\right)+6\,^{232}F_T\,^{232}Th\left(e^{\lambda_{232}t}-1\right)+^{147}F_T\,^{147}Sm\left(e^{\lambda_{147}t}-1\right)$$

100 (2)

We refer to dates calculated with this correction applied as "alpha-ejection corrected" or simply "corrected" dates, while dates calculated with no correction applied using Eq. (1) we refer to as "uncorrected" or "raw" dates.

For this work, it is assumed that the amount and uncertainty of each nuclide has been constrained. The natural U isotopic ratio (137.818 ± 0.023 1s; Hiess et al., 2012) is usually used to calculate ^{235}U in a sample based on the ^{238}U amount
105 measured. In these cases, the uncertainty in ^{235}U is perfectly correlated with ^{238}U; treatment of these uncertainties as though they were independent could lead to inaccurate uncertainty calculations. Whether or not the uncertainty in the other radionuclides is correlated depends on the details of isotope spiking procedures and must be evaluated on an individual lab basis. The option to incorporate correlated radionuclide uncertainty is included in the methods for propagating uncertainty.

Uncertainty and systematic error in F_T values likely stems from a combination of inaccurate grain measurements,
110 assumptions regarding the specific geometry of a given grain (i.e., deviations from the "idealized" shapes in Ketcham et al., 2011), and undetected parent nuclide zonation (Farley et al., 1996). When the magnitudes of these effects are constrained then the corresponding uncertainties can be propagated into the F_T value uncertainty and F_T values can be corrected for systematic error. Several approaches have been developed to approximate the 3D shape of individual grains to assess uncertainty associated with grain geometry estimates, generally finding that geometric uncertainty in F_T ranges between 2-
115 8% (1s) (Cooperdock et al., 2019; Evans et al., 2008; Glotzbach et al., 2019; Herman et al., 2007; Zeigler et al., 2022). The magnitude of systematic error depends on grain shape and the details of the method used for F_T value determination (e.g., Cooperdock et al., 2019; Glotzbach et al., 2019; Zeigler et al., 2022). Measurement of parent nuclide zonation is not currently done in typical workflows, so this source of uncertainty in F_T is generally unquantified, but it could be included in F_T uncertainty in the future if labs characterize zonation prior to dating. The isotope-specific F_T values are highly correlated
120 (Zeigler et al., 2022), so we include correlated F_T uncertainty in the methods below.

Several additional sources of dispersion in (U-Th)/He dates exist, including alpha implantation (e.g., Murray et al., 2014) and the influence of defects on He diffusion (e.g., Zeitler et al., 2017). These factors potentially contribute to intra-sample variability, but would not cause dispersion in repeated measurements of the same grain, and thus are best considered as part of multi-aliquot data compilations.

125 **3 Date and uncertainty calculation methods**

Here, (U-Th)/He dates are calculated by first estimating a date using an approximation of the helium age equation that solves directly for time. Using this estimate as an initial value, the exact date is then calculated iteratively using the Newton-Raphson method. We describe two independent methods (linear uncertainty propagation and Monte Carlo uncertainty modeling) of calculating the uncertainty in this date given the uncertainty components described in Sect. 2
130 above. We exclusively use the term "linear uncertainty propagation" rather than "analytical" or "standard" propagation to avoid confusion with analytical error arising from instrument noise and standards used in analytical measurements,

respectively. The linear method allows precise and repeatable calculations, while the Monte Carlo method is slightly more accurate and allows for calculation of skewed probability distributions, as discussed further in section 5.

3.1 Date calculation

135   The initial value for iterative age calculation is obtained by calculating an approximated noniterative solution of the (U-Th)/He age equation as described by Meesters and Dunai (2005). We slightly modify the production term in this method to permit calculation of parent-specific alpha ejection-corrected effective helium production rates:

$$p_j = N \times {}^jF_T \times \lambda_j \times {}^jM$$

(3)

140   Where p_j is the ^{4}He production rate, N is the number of alpha particles produced by a given decay chain, and ${}^jF_T$, λ_j, and ${}^jM$ are the alpha ejection-correction factor, decay constant, and concentration of radionuclide j (i.e. ${}^{238}U$, ${}^{235}U$, ${}^{232}Th$, and ${}^{147}Sm$), respectively.

Using the resulting date approximation as an initial guess (t_0), the (U-Th)/He date is then found using the relatively simple but highly efficient Newton-Raphson method

145

$$t_{i+1} = t_i - \frac{f(t_i)}{f'(t_i)}$$

(4)

$$f(t_i) = 0 = \left[\sum_{j=1}^{4} N \, {}^jF_T \, {}^jM\left(e^{\lambda_j t_i} - 1\right)\right] - He$$

(5)

$$t_{i+1} = t_i - \frac{\left[\sum_{j=1}^{4} N \, {}^jF_T \, {}^jM\left(e^{\lambda_j t_i} - 1\right)\right] - He}{\sum_{j=1}^{4} N\lambda_j \, {}^jF_T \, {}^jMe^{\lambda_j t_i}}$$

150   (6)

where t_i and t_{i+1} are successive approximations of the date, and $f(t_i)$ and $f'(t_i)$ are the implicit age equation (the helium age equation set at zero; Eq. (5)) and its first derivative with respect to t, respectively. This calculation is repeated until the difference between successive iterations is less than one year. This method benefits from an accurate initial guess and a quadratic rate of convergence such that generally only three to five iterations are required, though for dates >500 Ma (where
155   the noniterative approximation produces relative errors of >0.1% ; Meesters and Dunai, 2005), as many as ten iterations may be needed.

3.2 Linear uncertainty propagation

Here we provide a method of calculating date uncertainty using linear propagation of uncertainty. We apply the general formula for uncertainty propagation through a function $f(a, b…z)$, including cross terms for correlated error where
160   such correlations exist (Bevington and Robinson, 2003):

$$\sigma_f = \sqrt{\left(\frac{\partial f}{\partial a}\sigma_a\right)^2 + \left(\frac{\partial f}{\partial b}\sigma_b\right)^2 + 2\frac{\partial f}{\partial a}\frac{\partial f}{\partial b}\sigma_{ab}{}^2 + \cdots + \left(\frac{\partial f}{\partial z}\sigma_z\right)^2}$$

(7)

The following equations presume that ^{235}U has not been measured directly, but equations that include directly quantified ^{235}U are provided in Appendix A, and the HeCalc software released with this paper includes an option to account for either means of constraining ^{235}U. As an alternative to the use of HeCalc, these equations could be replicated in spreadsheet programs with a one-time expenditure of effort.

Applying the uncertainty propagation equation to the (U-Th)/He age equation, including potential covariance in the radionuclide and F_T uncertainties (i.e., the potential that the uncertainties are not fully independent), indicates that the uncertainty in a (U-Th)/He date is:

$$\sigma_t = \sqrt{\begin{aligned} & \left(\frac{\partial t}{\partial\,^4He}\sigma_{He}\right)^2 + \left(\frac{\partial t}{\partial^{238}U}\sigma_{238}\right)^2 + \left(\frac{\partial t}{\partial^{232}Th}\sigma_{232}\right)^2 + \left(\frac{\partial t}{\partial^{147}Sm}\sigma_{147}\right)^2 + \\ & 2\frac{\partial t}{\partial^{238}U}\frac{\partial t}{\partial^{232}Th}\sigma_{238-232}{}^2 + 2\frac{\partial t}{\partial^{238}U}\frac{\partial t}{\partial^{147}Sm}\sigma_{238-147}{}^2 + 2\frac{\partial t}{\partial^{232}Th}\frac{\partial t}{\partial^{147}Sm}\sigma_{232-147}{}^2 + \\ & \left(\frac{\partial t}{\partial^{238}F_T}\sigma_{Ft238}\right)^2 + \left(\frac{\partial t}{\partial^{235}F_T}\sigma_{Ft235}\right)^2 + \left(\frac{\partial t}{\partial^{232}F_T}\sigma_{Ft232}\right)^2 + \left(\frac{\partial t}{\partial^{147}F_T}\sigma_{Ft147}\right)^2 + \\ & 2\frac{\partial t}{\partial^{238}F_T}\frac{\partial t}{\partial^{235}F_T}\sigma_{Ft238-Ft235}{}^2 + 2\frac{\partial t}{\partial^{238}F_T}\frac{\partial t}{\partial^{232}F_T}\sigma_{Ft238-Ft232}{}^2 + \\ & 2\frac{\partial t}{\partial^{238}F_T}\frac{\partial t}{\partial^{147}F_T}\sigma_{Ft238-Ft147}{}^2 + 2\frac{\partial t}{\partial^{235}F_T}\frac{\partial t}{\partial^{232}F_T}\sigma_{Ft235-Ft232}{}^2 + \\ & 2\frac{\partial t}{\partial^{235}F_T}\frac{\partial t}{\partial^{147}F_T}\sigma_{Ft235-Ft147}{}^2 + 2\frac{\partial t}{\partial^{232}F_T}\frac{\partial t}{\partial^{147}F_T}\sigma_{Ft232-Ft147}{}^2 \end{aligned}}$$

(8)

where, for example, σ_{He} is the uncertainty in the ^{4}He measurement, and $\sigma_{238-232}$ is the covariance between ^{238}U and ^{232}Th. Note that the covariance terms collapse to 0 if no correlation exists between uncertainties, while positive covariance will increase the overall uncertainty.

While solving the (U-Th)/He age equation for t explicitly is not possible, finding the first derivative of t with respect to each variable is possible through implicit differentiation. Specifically,

$$\frac{\partial t}{\partial X} = -\frac{\frac{\partial f}{\partial X}}{\frac{\partial f}{\partial t}}$$

(9)

where X is each variable in the (U-Th)/He age equation with an uncertainty. Using this relationship, the relevant derivatives are:

$$\frac{\partial f}{\partial\,^4He} = \frac{1}{\sum_{j=1}^4 N\lambda_j\,^jF_T\,^jMe^{\lambda_j t_i}}$$

(10)

$$\frac{\partial f}{\partial^{238}U} = -\frac{8^{238}F_T\left(e^{\lambda_{238}t_i}-1\right) + \frac{7}{137.818}\,^{235}F_T\left(e^{\lambda_{235}t_i}-1\right)}{\sum_{j=1}^4 N\lambda_j\,^jF_T\,^jMe^{\lambda_j t_i}}$$

(11)

185

$$\frac{\partial f}{\partial^{232}Th} = -\frac{6\,^{232}F_T\left(e^{\lambda_{232}t_i}-1\right)}{\sum_{j=1}^{4} N\lambda_j\,^jF_T\,^jMe^{\lambda_j t_i}}$$

(12)

$$\frac{\partial f}{\partial^{147}Sm} = -\frac{^{147}F_T\left(e^{\lambda_{147}t_i}-1\right)}{\sum_{j=1}^{4} N\lambda_j\,^jF_T\,^jMe^{\lambda_j t_i}}$$

(13)

$$\frac{\partial f}{\partial\,^jF_T} = -\frac{N\,^jM\left(e^{\lambda_j t_i}-1\right)}{\sum_{j=1}^{4} N\lambda_j\,^jF_T\,^jMe^{\lambda_j t_i}}$$

190   (14)

Where each summation term involves addition of the four radionuclides with the same variable convention described in Sect. 2.1.1 above and $\frac{^{238}U}{137.818}$ used in place of ^{235}U, e.g.:

$$\sum_{j=1}^{4} N\lambda_j\,^jF_T\,^jMe^{\lambda_j t_i} = \left[\begin{array}{l} 8\lambda_{238}\,^{238}F_T\,^{238}Ue^{\lambda_{238}t_i} + \dfrac{7}{137.818}\lambda_{235}\,^{235}F_T\,^{238}Ue^{\lambda_{235}t_i} + \\ 6\lambda_{232}\,^{232}F_T\,^{232}The^{\lambda_{232}t_i} + \lambda_{147}\,^{147}F_T\,^{147}Sme^{\lambda_{147}t_i} \end{array}\right]$$

(15)

195   These equations are printed in their expanded forms, along with versions that allow for direct quantification of ^{235}U, in Appendix A.

3.3 Monte Carlo uncertainty 6odelling

        Monte Carlo uncertainty propagation is based on the approach of combining the uncertainty in measured parameters with any given probability distribution (including non-gaussian distributions as may be caused by compositional zoning;
200   Hourigan et al., 2005) by randomly sampling each distribution a large number of times and propagating those randomly generated parameters through some function of interest (Eqs. (7) and (10); Fig. 1). This method yields a probability density histogram that describes the true uncertainty to arbitrary precision depending on the number of simulations run (Anderson, 1976; Efron and Tibshirani, 1986; Possolo and Iyer, 2017). As such, the application of Monte Carlo techniques is mathematically straightforward, in this case requiring no knowledge beyond that required to calculate a (U-Th)/He date. In
205   addition to this benefit, Monte Carlo uncertainty analysis does not require that a function of interest have a linear first term of the Taylor series to accurately calculate uncertainty; when this assumption is violated (as in the (U-Th)/He age equation), uncertainties propagated using linear uncertainty propagation (Eq. (7)) can be inaccurate. Future work may also permit analysis of the effects of non-linear input uncertainties to date uncertainty. While the Monte Carlo method has historically been hindered by computational expense, the increases in computational power in recent decades make this more accurate
210   approach an attractive method for routine uncertainty propagation in (U-Th)/He chronology.
        Here, Monte Carlo uncertainty modeling of (U-Th)/He data is performed by generating arrays of a pre-determined size N, which contain randomly generated values for each input according to the gaussian distribution described by each value's 1σ uncertainty (Fig. 1, input probability distributions). Correlated uncertainties (correlations between ^{238}U, ^{232}Th, and ^{147}Sm, and also between $^{238}F_T$, $^{235}F_T$, $^{232}F_T$, and $^{147}F_T$) are generated using multivariate gaussian distributions according to a
215   covariance matrix consisting of each value's 1σ uncertainty and the covariance term for each pair of variables. Arrays of raw and corrected dates (including any non-physical negative dates calculated; Appendix B) of size N are then calculated as

described above using these randomly generated variables. From these arrays, 68% and 95% confidence intervals are calculated using the 15.865 and 84.135, and 2.275 and 97.725 percentiles of the samples of dates, respectively. We use confidence intervals as opposed to standard deviation because some output uncertainty distributions are skewed. Although the average of the 68% and 95% confidence intervals yields the 1- and 2-standard deviation levels for reasonably gaussian (normal) distributions, this does not necessarily hold for non-gaussian (asymmetric or skewed) distributions (Fig. 1, example output probability distributions).
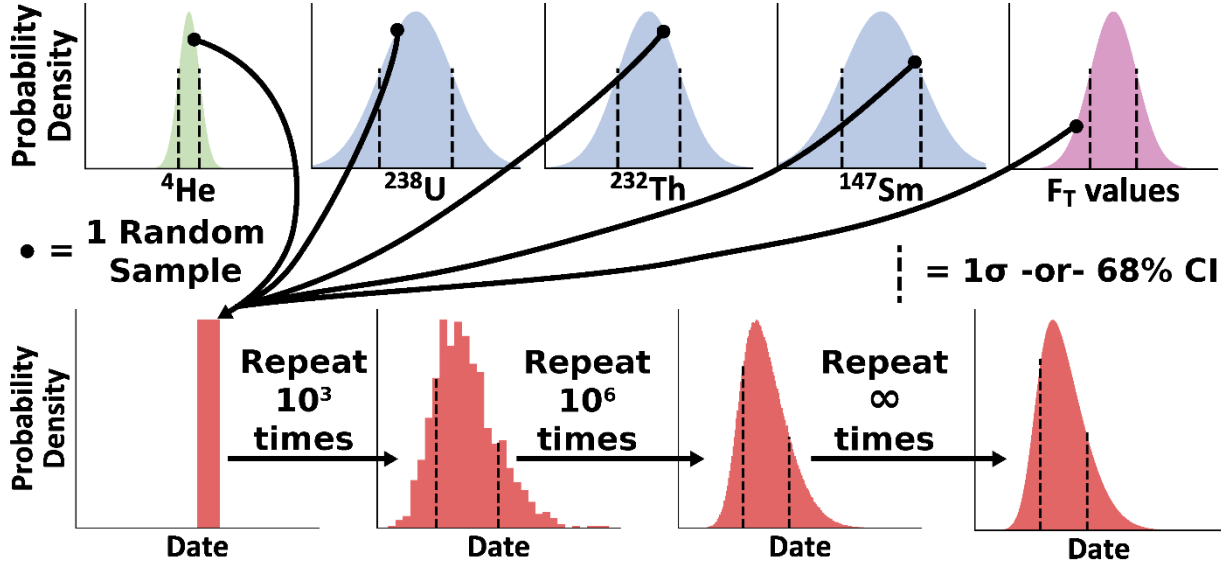
Figure 1: A conceptual diagram of Monte Carlo uncertainty modeling for the (U-Th)/He system. Each independent gaussian input probability distribution (with 1σ standard deviation marked as vertical lines) is sampled at random a large number of times. Because we assume fully correlated F_T uncertainties, the isotope-specific F_T distributions are represented by a single distribution where an individual percent deviation from the mean value is sampled four times. Using these randomly sampled inputs, a single date is calculated. This process is repeated until the probability distribution of interest (in this case, a skewed non-gaussian distribution with the 68% confidence interval shown with vertical lines) has been sufficiently sampled, as set by the analyst.

The number of Monte Carlo simulations dictates the precision of the results because Monte Carlo analysis is a numerical approximation of uncertainty, (e.g., the lower panels in Fig. 1 become progressively smoother with an increasing number of simulations). Therefore, separate from the probability distribution describing date uncertainty, there is a predictable level of variation in uncertainty estimates and other parameters describing the probability distribution (e.g., its mean) given a certain number of total Monte Carlo simulations (Wübbeler et al., 2010). Specifically, the standard error of the standard deviation of a Monte Carlo model is dependent on the uncertainty in the value itself and the number of simulations:

$$\sigma_\mu = \frac{\sigma_t}{\sqrt{2N-2}}$$

(16)

where σ_μ is the standard deviation of the population mean, σ_t the date uncertainty, and N the number of simulations. To avoid running arbitrary numbers of simulations, we invert this equation to determine the number of iterations required to achieve a user-requested relative precision on the mean:

$$\sigma_\mu \sim (\bar{x} \times p)$$

(17)

$$N = \frac{2(\bar{x} \times p)^2 + \sigma_t{}^2}{2(\bar{x} \times p)^2}$$

245 (18)

Where N is the number of simulations to run, σ_t is the date uncertainty estimated by linear uncertainty propagation, $\bar{x}$ is the sample mean estimated by calculation of the date using the nominal input values, and p is the user-requested precision in percent uncertainty. By using percent relative uncertainty, the value of the date itself need not be known *a priori*, as an estimate of the standard deviation of the population mean date can be calculated using the percent relative precision and the

250 date calculation from the input values (Eq. (18)).

4 Helium date and uncertainty Calculator (HeCalc) code

In this section we describe the implementation of the above methods of date and uncertainty calculation in the new HeCalc software (Martin, 2022). For ease of access and to best provide this software as a resource to the helium community, HeCalc is available both as a standalone program with a graphical user interface (GUI) and as a package in Python 3

255 available for download from the Python Package Index (PyPI) via pip commands. The descriptions below apply specifically to the GUI version of the software and the main_hecalc() function in the Python package; those interested in writing their own code and incorporating the component functions provided in HeCalc may consult the associated documentation for more detailed programming considerations.

4.1 Input

260 The input for HeCalc is designed to be straightforward and flexible (Table 1). Input files may be in Excel (.xls/.xlsx), comma separated value (.csv), or tab-delimited text (.txt) format. In addition to data input through a file, HeCalc users may manually input values to calculate a date and uncertainty for a single set of data by clicking on the "Manual" tab. If importing data through a file, the file must contain columns for sample name, U, Th, Sm, He, and all F_Ts with the headers Sample, mol 238U, mol 232Th, mol 147Sm, mol 4He, 238Ft, 235Ft, 232Ft, and 147Ft (Table 1). Although "mol X" is

265 required as the input column header for U, Th, Sm, and He, the actual units of the input data may be any unit of quantity (e.g., atoms, mol/g, etc.) as long as they are identical. The 1σ uncertainty for each value, in the same units, must be included in the column following each respective value, even if the applied uncertainty is 0 (e.g., for F_T values with unknown uncertainty); there is no naming requirement for these headers. If ^{235}U was measured directly, columns for this measurement and its uncertainty should also be present. Correlated uncertainty between the radionuclides and between the isotope-specific

270 F_T values can be input using their Pearson correlation coefficient, which is related to the covariance as:

$$r_{ab} = \frac{\sigma_{ab}{}^2}{\sigma_a \sigma_b}$$

(19)

where σ_{ab} is the covariance between variables a and b. The correlation coefficient is preferable to inputting covariance directly as it has the intuitive meaning of being in the range of [-1, 1] where 1 is perfectly correlated and 0 is fully

275 uncorrelated, while numerical covariance is generally unintuitive. These values may be included in the input file using headers with the naming convention "r 238U-235U" and "r 238Ft-235Ft" (Table 1); either ordering of the correlated uncertainties in the header (i.e., "r 238U-235U" vs. "r 235U-238U") is permitted. Uncertainties are assumed to be uncorrelated unless these columns are explicitly included. Example input files both with and without correlated uncertainty are provided as templates in the code's repository (see the Code availability Section for a direct link).

280 The order in which these columns appear is unimportant as long as the uncertainty associated with each value follows that value. Extraneous columns with differing headers also will not interfere with the code's execution. Additionally, if an input Excel file has multiple sheets, the first sheet will be read in by default. If this sheet does not contain the required

column headers, the program will ask for the name of the sheet to use instead. In this way, HeCalc ideally allows for input of any given lab's standard data reduction spreadsheet or other typical data product with no or minimal alteration, allowing it to
285 be integrated seamlessly into a lab's existing workflow.

In addition to data input, several further options are provided. The number of decimals included in the output is determined by the user (this option affects only output and does not impact the statistical aspects of the code). The user can also select whether to perform linear uncertainty propagation, Monte Carlo uncertainty propagation, both, or neither. If Monte Carlo uncertainty propagation is selected, the desired precision of the mean is specified in percent as described above.
290 In practice, the precision of the mean date need be no better than the number of significant figures present the in data; for common (U-Th)/He analyses, this equates to a precision of ~0.01%, which generally requires on the order of 10^4-10^5 simulations. The program also contains the ability to generate histograms using the Monte Carlo results. If this option is chosen, this histogram may be parameterized as a skew-normal distribution (Azzalini and Capitanio, 1999; O'Hagan and Leonard, 1976).
295

Table 1. Example HeCalc inputs.[a]

Column header	Example required data input
Sample	Sample1
mol 4He	0.1
±	0.001
mol 238U	1
±	0.05
mol 232Th	1
±	0.05
mol 147Sm	1
±	0.05
238Ft	0.7
±	0.05
235Ft	0.7
±	0.05
232Ft	0.7
±	0.05
147Ft	0.7
±	0.05
Column header	**Example optional data input**
r 238U-232Th[b]	0.1
r 238U-147Sm	0.1
r 232Th-147Sm	0.1
r 238Ft-235Ft	0.9
r 238Ft-232Ft	0.9
r 238Ft-147Ft	0.9
r 235Ft-232Ft	0.9
r 235Ft-147Ft	0.9
r 232Ft-147Ft	0.9

4.2 Output

There are two main outputs from HeCalc: the results of the date calculation and uncertainty propagation, and the histograms of the Monte Carlo results for each sample (Table 2). At a minimum, the sample name, raw date, and corrected

300 date are saved to an Excel sheet titled "Uncertainty Output" that includes a header with the input file's name and directory. The raw and corrected dates in these columns are calculated using each exact input value (e.g., mol 238U = 1 in Table 1); we refer to these dates as "nominal dates" below. The selection of linear uncertainty propagation causes columns to be added titled "Linear raw 1σ uncertainty", "Linear raw 2σ uncertainty", "Linear corrected 1σ uncertainty", and "Linear corrected 2σ uncertainty", with "raw" indicating no alpha ejection correction. If Monte Carlo error propagation is selected, a header line

305 specifying the user-requested precision is added, and the columns "MC average 68% CI, raw", "MC +68% CI, raw", "MC -68% CI, raw", "MC average 95% CI, raw", "MC +95% CI, raw", "MC -95% CI, raw", and the corresponding values for F_T-corrected dates (titled with "corrected" instead of "raw") are included along with a column giving the number of Monte Carlo simulations run. The confidence intervals are reported as the 15.865 and 84.135 percentiles (the 68% confidence interval) and the 2.275 and 97.725 percentiles (the 95% confidence interval) of the Monte Carlo results, converted to

310 uncertainty values by reference to the nominal date. Throughout this manuscript, the asymmetry of the confidence intervals will be calculated with respect to the nominal date calculation. It is worth noting that the nominal date does not strictly correspond to the mode of the histogram, and instead falls toward the skewed side, meaning that the skew calculations presented here are a slight underestimate of the actual asymmetry in the distribution.

If the user chooses to include histograms in the output, an Excel sheet titled "Histogram Output" is added to the

315 workbook, with columns for the center of each histogram bin (i.e., the individual intervals in the histogram) and number of simulations in that bin as x- and y- values for the both the raw and F_T-corrected dates. Four total columns are therefore present for each sample. The number of bins is equal to 1/1000th the number of simulations run or ten bins, whichever is greater. If parameterization is selected, the histogram is fit to a skew-normal distribution. Although this distribution does not perfectly replicate the histograms generated by HeCalc, it allows for first-order interpretations using continuous probability

320 distributions. Columns are appended to the end of the "Uncertainty Output" sheet titled "Hist raw fit a", "Hist raw fit u", "Hist raw fit s", and the corresponding values for F_T-corrected calculations. These parameters correspond to the shape ("a", the skewness), location ("u", a measure of central tendency), and scale ("s", the width of the distribution) parameters for a skew-normal probability distribution function (Azzalini, 1985; O'Hagan and Leonard, 1976).

325

Table 2. Example HeCalc outputs, produced by Table 1 inputs

Output Header[a]	Example output:	Included when:
Sample	Sample1	Always
Raw date	62.4	Always
Linear raw 1σ uncertainty	2.7	Linear propagation selected
MC average 68% CI, raw	2.7	Monte Carlo propagation selected

MC +68% CI, raw	2.8	Monte Carlo propagation selected
MC -68% CI, raw	2.6	Monte Carlo propagation selected
Linear 2σ uncertainty, raw	5.4	Linear propagation selected
MC average 95% CI, raw	5.5	Monte Carlo propagation selected
MC +95% CI, raw	5.9	Monte Carlo propagation selected
MC -95% CI, raw	5.0	Monte Carlo propagation selected
Corrected date	89.0	Always
Linear 1σ uncertainty, corrected	7.3	Linear propagation selected
MC average 68% CI, corrected	7.4	Monte Carlo propagation selected
MC +68% CI, corrected	7.9	Monte Carlo propagation selected
MC -68% CI, corrected	6.8	Monte Carlo propagation selected
Linear 2σ uncertainty, corrected	14.6	Linear propagation selected
MC average 95% CI, corrected	14.9	Monte Carlo propagation selected
MC +95% CI, corrected	16.9	Monte Carlo propagation selected
MC -95% CI, corrected	12.8	Monte Carlo propagation selected
Number of Monte Carlo simulations	336352	Monte Carlo propagation selected
Hist raw fit a[b]	1.38	Parameterization selected (requires Monte Carlo)
Hist raw fit u[b]	60.2	Parameterization selected (requires Monte Carlo)
Hist raw fit s[b]	3.59	Parameterization selected (requires Monte Carlo)
Hist corrected fit a	1.77	Parameterization selected (requires Monte Carlo)
Hist corrected fit u	82.4	Parameterization selected (requires Monte Carlo)
Hist corrected fit s	10.31	Parameterization selected (requires Monte Carlo)

[a] The header for the file will contain a line for the file path of the input file and (if Monte Carlo propagation is selected) the user-requested precision.

b "Hist fit a" refers to the shape or skewness of the histogram. "Hist fit u" is a measure of central tendency of the histogram. "Hist fit s" is a measure of the width of the distribution. (Azzalini, 1985; O'Hagan and Leonard, 1976).

5 Discussion

Here we use the methods described above to calculate the dates and uncertainties for a compilation of real apatite and zircon (U-Th)/He data, and then examine the overall uncertainty budget and skew in this dataset. In the appendices we additionally explore the influence of theoretical input uncertainties on date uncertainty, on skew in Monte Carlo date distributions, and on the differences in dates derived from the linear and Monte Carlo methods (Appendices C-E).

5.1 Uncertainty budget in real data

To assess the uncertainty budget in real (U-Th)/He data, we compiled 1,978 apatite and 1,753 zircon analyses that were acquired with typical and consistent (U-Th)/He methods and instrumentation (quadrupole noble gas mass spectrometer and quadrupole ICP-MS) in the University of Colorado Thermochronology Research and Instrumentation Laboratory (CU TRaIL). These data were measured from October 2017 to March 2020 following the methods described in Sturrock et al. (2021) for apatite and Peak et al. (2021) for zircon. Figure 2 shows the histograms of percent relative uncertainty in the absolute amounts of ^{4}He, ^{238}U, ^{232}Th, and (for apatite) ^{147}Sm for this dataset, while Table 3 lists the median value and 68% confidence interval calculated using the percentile approach (Sect. 3.3) for these distributions. Analytical uncertainties are typically higher for apatites than for zircons due to the lower ^{4}He and radionuclide amounts for apatites relative to zircons, which causes apatite measurements to have lower count rates that are more impacted by blank and background uncertainties. For both apatite and zircon analyses, radionuclide uncertainties are higher than ^{4}He uncertainties. For example, for apatites, the percent uncertainties in ^{238}U, ^{232}Th, and ^{147}Sm amounts are 3.2%, 2.8%, and 2.8%, respectively, which are 3-4x less precise than the uncertainty in the ^{4}He amount of 0.86% (Fig. 2a; Table 3). For zircons, the uncertainties of ^{238}U and ^{232}Th are 1.8% and 2.2%, respectively, which are 5-6.5x less precise than the ^{4}He uncertainty of 0.34% (Fig. 2b, Table 3).
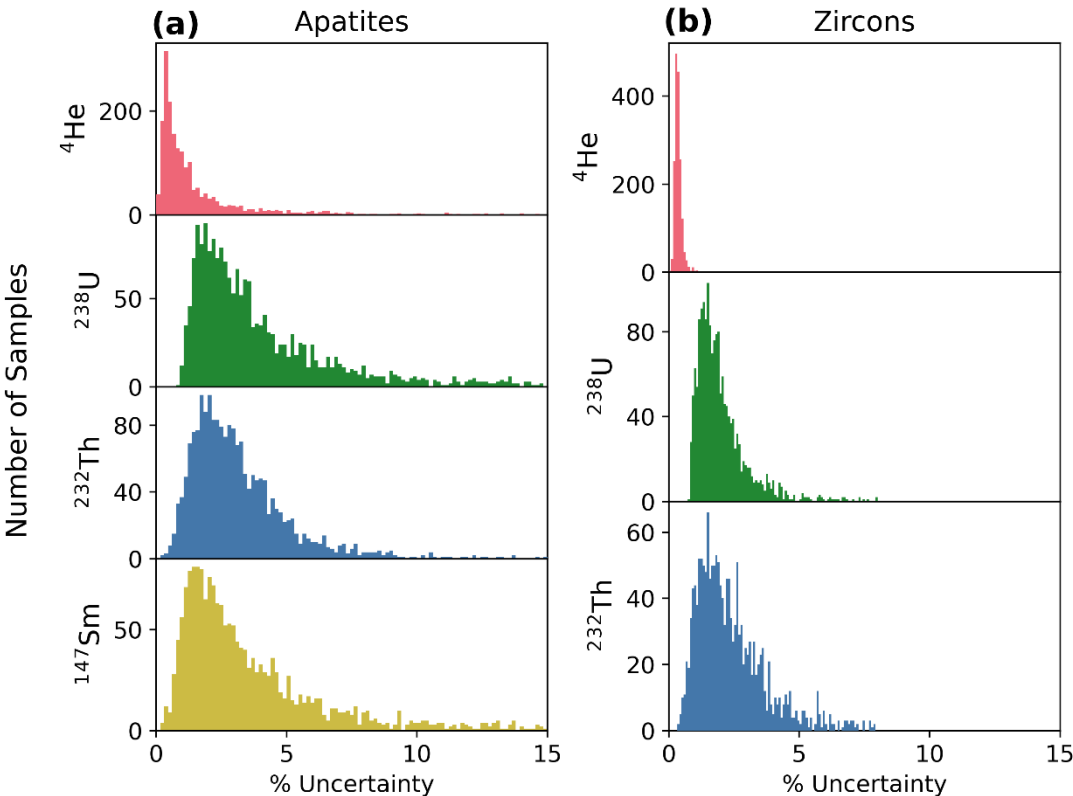
Figure 2: Histograms of percent relative uncertainty in ⁴He, ²³⁸U, ²³²Th, and ¹⁴⁷Sm absolute amounts for (a) apatite (N = 1,978) and (b) zircon (N = 1,753). Note that the y-axis scales differ for these plots.

Table 3. Percent uncertainties on absolute amounts of ⁴He and radionuclides for apatite and zircon analyses in data compilation.

⁴He or radionuclide	Apatite (n = 1,978)	Zircon (n = 1,753)
	Uncertainty on absolute amount (%)[a]	Uncertainty on absolute amount (%)[a]
⁴He	0.86 [+1.9, -0.51]	0.34 [+0.14, -0.10]
²³⁸U	3.2 [+3.6, -1.4]	1.8 [+1.1, -0.6]
²³²Th	2.8 [+2.0, -1.2]	2.2 [+2.3, -1.0]
¹⁴⁷Sm	2.8 [+4.4, -1.4]	N.M.[b]

[a]Data reported as median and 68% confidence intervals

[b] N.M. = Not Measured

350

We analyze the uncertainty in these data with and without propagating F_T uncertainty using HeCalc (Fig. 3). For illustrative purposes, we explored two different scenarios assuming 2% and 5% uncertainties in the isotope-specific F_T values and fully correlated F_T uncertainties. These uncertainties are based on those reported by Zeigler et al. (2022), which found that the F_T uncertainty depends partly on grain geometry. Figure 3 shows the distributions of percent relative
355 uncertainty calculated by the Monte Carlo method for the apatite and zircon corrected (U-Th)/He dates. Table 4 lists the median value and 68% confidence interval for these distributions. Propagating only analytical uncertainties (on radionuclides and ⁴He) yields median date uncertainties of 2.9% and 1.7% for apatite and zircon, respectively. With uncertainty in F_T included, the date uncertainty increases substantially. For apatites, the uncertainty value increases from 2.9% for analytical uncertainties alone to 3.5% and 5.8%, respectively, when F_T uncertainties of 2% or 5% are also propagated. For zircons, the
360 uncertainty increases from 1.7% to 2.6% and 5.2%, respectively. The addition of F_T uncertainty most heavily impacts the analyses with more precise radionuclide and ⁴He measurements because F_T uncertainty comprises a correspondingly larger proportion of the uncertainty budget. Given that F_T geometric uncertainty estimates are on the same order of magnitude as— and in some cases larger than—typical analytical uncertainties in (U-Th)/He dating, additional efforts to constrain F_T uncertainty (i.e., on minerals other than apatite, such as zircon) are important to rigorously calculate uncertainties in
365 individual (U-Th)/He dates.
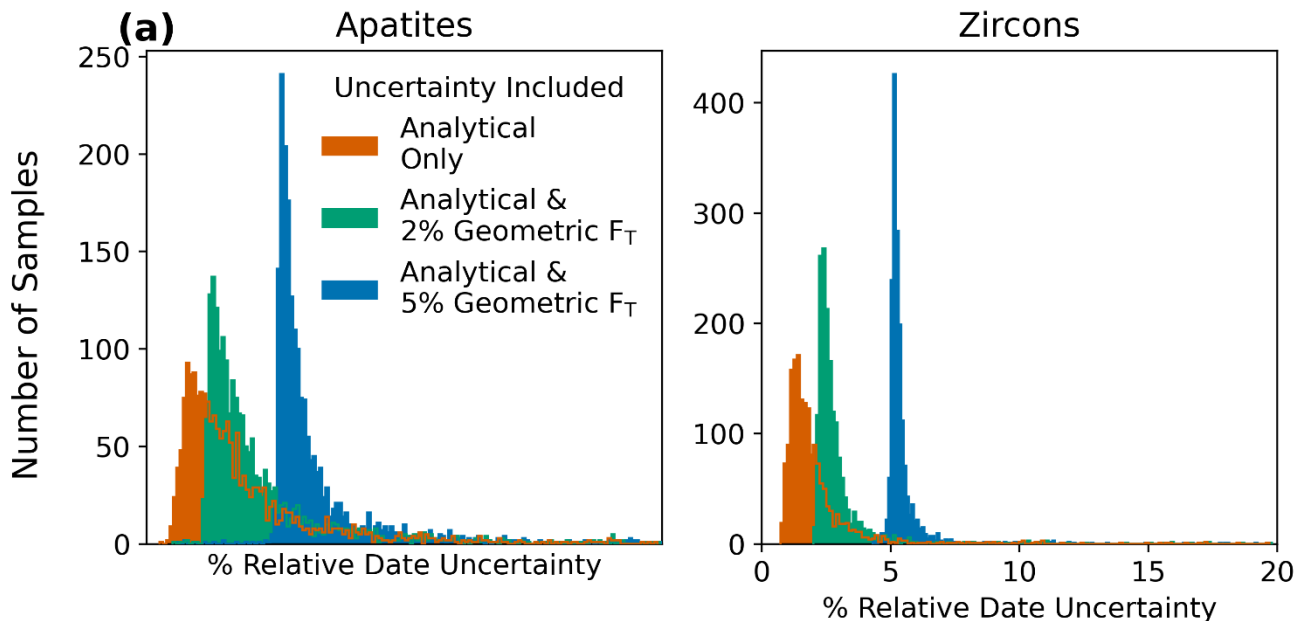
Figure 3: Histograms of percent relative uncertainty for corrected (U-Th)/He dates for (a) apatite (N = 1,978) and (b) zircon (N = 1,753) analyses. The top panels show input uncertainties for only analytical uncertainties (^{4}He and radionuclides), while the lower panels additionally include 2% or 5%geometric uncertainties in F_T. Calculations assume fully correlated isotope-specific F_T uncertainties ($r = 1$) based on Zeigler et al. (2022), and assume fully uncorrelated radionuclide uncertainties for these radionuclide data.

Table 4. Percent uncertainty on corrected (U-Th)/He dates, percent skew of Monte Carlo-generated date distributions, and percent error in linear propagation method for apatite and zircon analyses in data compilation.

Propagated Uncertainty Components	Apatite (n = 1,978)			Zircon (n = 1,753)		
	Corrected (U-Th)/He Date Uncertainty (%)[b]	Skew (%)[b,c]	Linear Propagation Error (%)[b,d]	Corrected (U-Th)/He Date Uncertainty (%)[b]	Skew (%)[b,c]	Linear Propagation Error (%)[b,d]
Analytical Only[a]	2.9 [+3.1, -1.2]	4.4 [+4.3, -2.0]	-0.064 [+0.05, -0.14]	1.7 [+1.1, -0.5]	3.2 [+2.3, -1.0]	-0.035 [+0.037, -0.059]
Analytical & 2% F_T	3.5 [+2.8, -0.9]	6.0 [+3.7, -1.4]	-0.11 [+0.057, -0.13]	2.6 [+0.8, -0.3]	5.2 [+1.6, -0.6]	-0.080 [+0.040, -0.053]
Analytical & 5% F_T	5.8 [+2.1, -0.5]	11.4 [+2.5, -0.8]	-0.31 [+0.057, -0.16]	5.2 [+0.5, -0.2]	11.0 [+0.9, -0.4]	-0.27 [+0.04, -0.06]

[a]Analytical refers to uncertainties in ^{4}He and radionunclides

[b]Data reported as median and 68% confidence intervals

[c]Skew is defined here as percent difference between the positive and negative 68% confidence intervals relative to the date.

[d]Percent difference between uncertainty derived from linear uncertainty propagation and averaged 68% confidence intervals from Monte Carlo uncertainty propagation.

375

5.2 Skew in real data

We also analyze the compilation of real data in Figure 2 for skew in Monte Carlo-generated date probability distributions (i.e., asymmetric uncertainty). Although "skewness" is a statistical concept referring to the third standardized moment of a population, this metric is unitless and generally unintuitive, so here we report skew by taking the percent
380 difference between the positive and negative 68% confidence intervals with respect to the date. Analysis of theoretical data reveals that skew increases with relative input uncertainty and varies with age (Appendix D; Fig. D1-D3). In our data compilation, positive skew is common and can be significant, as would be predicted based on the theoretical data analysis

and the real data uncertainties in Table 3. With only analytical uncertainty included, the median skew in apatites and zircons is 4.4% and 3.2%, respectively. The inclusion of F_T uncertainty increases the skew (Fig. 4a-b, Table 4). For apatites, skew
385 rises to 6.0% and 11.4% for 2% and 5% uncertainty in F_T, respectively (Fig. 4a, Table 4). For zircons, the same combinations of uncertainty yield skews of 5.2% and 11.0% (Fig. 4b, Table 4). For a 2% F_T uncertainty, ~14% of apatite data and ~5% of zircon data have a skew of 10% or greater. As an example, for 10% skew, a 100±6.4 Ma date would be represented as 100 [+6.7, -6.1] Ma at the 1s level.

General practice in (U-Th)/He dating has been to report symmetric uncertainties. Our analysis reveals that for most
390 cases this is appropriate, and averaging asymmetric uncertainties in data reporting is unlikely to substantially impact interpretations. However, for highly asymmetric uncertainties, it may be appropriate to report positive and negative uncertainties separately, and only combine the reported uncertainties if they are indistinguishable within the appropriate number of significant figures. Our results suggest that skew may be an important consideration when interpreting (U-Th)/He data with less precise [4]He and radionuclide measurements, because these data generally have date uncertainties with greater
395 skew. In these cases, asymmetric uncertainties may be important for determining whether a dataset is consistent with a given hypothesis within uncertainty. However, a challenge to interpreting dates with asymmetric uncertainties is that no widely used inverse thermal history modeling software for (U-Th)/He data permits asymmetric uncertainty input. Future work implementing skewed probability distributions in such software may enhance interpretation of the subset of (U-Th)/He data characterized by highly skewed uncertainties.

400
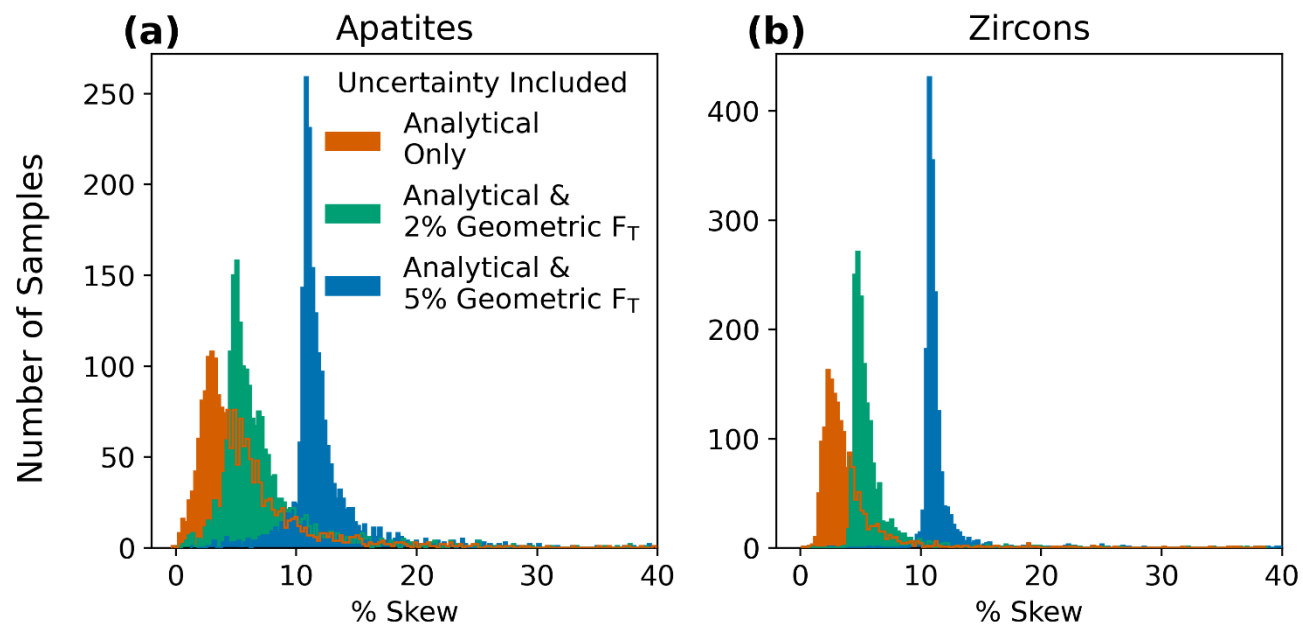
Figure 4: Histograms of skew as percent asymmetry in the 68% confidence intervals for (a) apatite (N = 1,978) and (b) zircon (N = 1,753) analyses. Input uncertainties include analytical uncertainty only ([4]He and radionuclides), and analytical uncertainties propagated with 2% or 5% geometric uncertainty in F_T, assuming fully correlated individual F_T uncertainty values (r = 1). The
405 **outlines of covered histograms are included to show detail for each. Note that the y-axis scales differ between the two plots.**

5.3. Comparison of linear and Monte Carlo uncertainty propagation results for real data
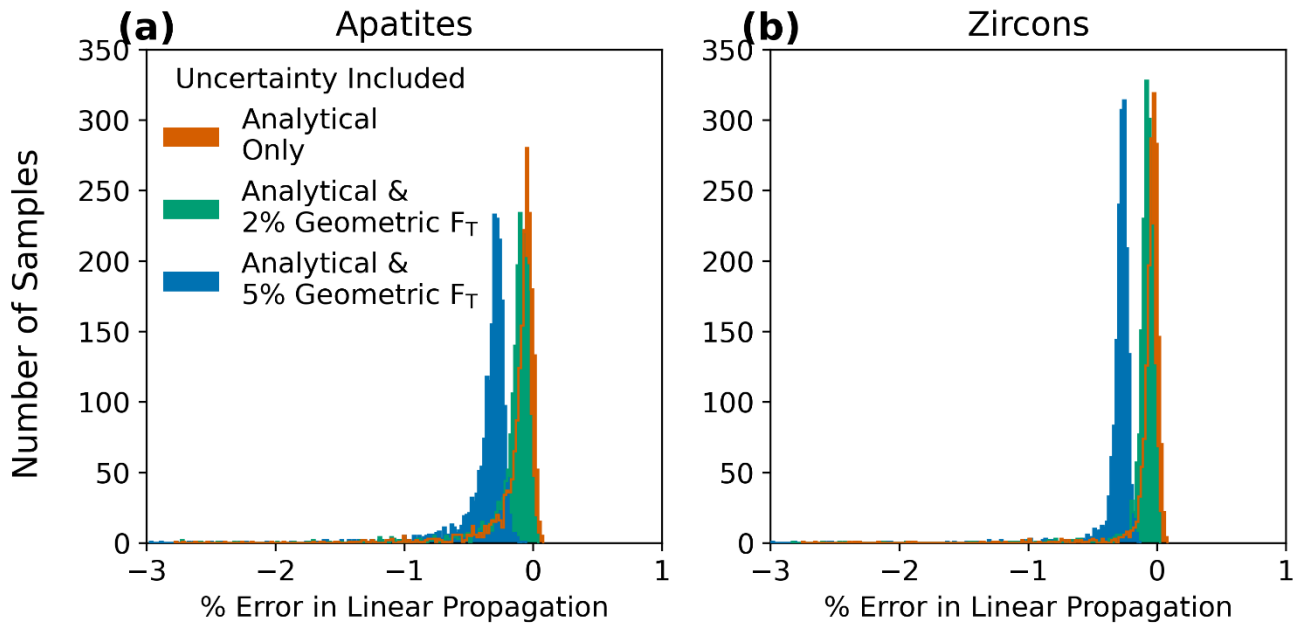
Figure 5: Histograms of the percent difference between averaged Monte Carlo-derived confidence intervals and linear uncertainty propagation for (a) apatite (N = 1,978) and (b) zircon (N = 1,753) analyses. Input uncertainties include analytical uncertainty only ([4]He and radionuclides), and analytical uncertainties propagated with 2% or 5% geometric uncertainty in F_T, assuming fully correlated individual F_T uncertainty values (r = 1). The outlines of covered histograms are included to show detail for each. Note that the y-axis scales differ between the two plots.

Finally, we compare the uncertainties derived from linear uncertainty propagation with the averaged 68% confidence intervals from Monte Carlo propagation for the compiled dataset. For nearly all analyses, the uncertainties yielded by the two methods are within 1% of each other, regardless of the amount of F_T uncertainty included (Fig. 5a, Table 4). Thus, error due to linear uncertainty propagation (i.e., inaccurately calculated uncertainty resulting from an assumption of linearity) is largely insignificant in this dataset, and the uncertainties yielded by the two methods are interchangeable in most circumstances. In contrast, skew, discussed in the previous section, is only revealed by the Monte Carlo method using the equations presented here and included in the HeCalc software. The asymmetric uncertainties of some samples, specifically those with atypically large input uncertainties, is more important for accurate uncertainty analysis than error introduced in the uncertainty calculation due to linear uncertainty propagation.

6 Conclusions

Here we publish fully traceable end-to-end calculations of uncertainty in (U-Th)/He dates, including the propagation of uncertainties in F_T values. We also provide a software package, HeCalc, to do these calculations explicitly and to perform more accurate Monte Carlo propagation of these uncertainties. Using a compilation of apatite and zircon (U-Th)/He analyses, we find that for a common instrumental setup (quadrupole noble gas and ICP mass spectrometers), uncertainty in radionuclide quantification is generally 3-6.5x larger than the uncertainty in [4]He measurement. When only [4]He and radionuclide uncertainties are propagated, the typical alpha ejection corrected (U-Th)/He date uncertainty is 2.9% for

apatites and 1.7% for zircons. The inclusion of 2% and 5% geometric uncertainty in the F_T values yields greater date uncertainty of 3.5% and 5.8% for apatites and 2.6% and 5.2% for zircons.

For the compiled dataset, the asymmetry in the 68% confidence interval can be significant, especially for dates with less precise input uncertainty. With 2% uncertainty included in F_T, 14% of all apatite and 5% of all zircon analyses have a
435 skew of greater than 10%. The results of linear uncertainty propagation for these data agree with those from Monte Carlo uncertainty propagation to within ~1%, indicating that this error is negligible. Given that Monte Carlo uncertainty propagation permits calculation of skewed probability distributions and does not make an assumption of linearity in the (U-Th)/He age equation, we propose that this method should be preferred for uncertainty calculation in (U-Th)/He data. However, the current lack of a means of including asymmetric uncertainty in thermal history modeling, and the roughly
440 equivalent symmetric uncertainty values from Monte Carlo and linear uncertainty propagation methods, indicates that the results are likely interchangeable for common workflows, pending advancements in the (U-Th)/He method and interpretative models.

The methods presented here allow for more rigorous inter-laboratory data comparisons and retrospective data analyses by providing a consistent means of quantifying the uncertainty budget of a given (U-Th)/He analysis. Further
445 developments of the (U-Th)/He technique are also facilitated by this study. In particular, this work suggests that continued refinement of F_T uncertainty is warranted, and provides a framework into which those developments may be placed. Using the Monte Carlo results, asymmetric uncertainty may also be quantified, and could potentially be included in future versions of thermal history modeling software. Finally, fully accounting for analytical and geometric uncertainties will better isolate the magnitude of overdispersion and promote more effective examination of its causes.

450 **Appendix A: Additional linear uncertainty propagation equations**

Here we print the equations presented in Sect. 3.2 in their expanded forms, along with a set of equations that allows for direct quantification of ^{235}U. First, the expanded form for each derivative is:

$$\frac{\partial f}{\partial\,^4He} = \frac{1}{\left[\begin{array}{c} 8\lambda_{238}\,^{238}F_T\,^{238}Ue^{\lambda_{238}t_i} + \frac{7}{137.818}\lambda_{235}\,^{235}F_T\,^{238}Ue^{\lambda_{235}t_i} + \\ 6\lambda_{232}\,^{232}F_T\,^{232}The^{\lambda_{232}t_i} + \lambda_{147}\,^{147}F_T\,^{147}Sme^{\lambda_{147}t_i} \end{array}\right]}$$

(a1)

455

$$\frac{\partial f}{\partial\,^{238}U} = -\frac{8\,^{238}F_T\left(e^{\lambda_{238}t_i} - 1\right) + \frac{7}{137.818}\,^{235}F_T\left(e^{\lambda_{235}t_i} - 1\right)}{\left[\begin{array}{c} 8\lambda_{238}\,^{238}F_T\,^{238}Ue^{\lambda_{238}t_i} + \frac{7}{137.818}\lambda_{235}\,^{235}F_T\,^{238}Ue^{\lambda_{235}t_i} + \\ 6\lambda_{232}\,^{232}F_T\,^{232}The^{\lambda_{232}t_i} + \lambda_{147}\,^{147}F_T\,^{147}Sme^{\lambda_{147}t_i} \end{array}\right]}$$

(a2)

$$\frac{\partial f}{\partial\,^{232}Th} = -\frac{6\,^{232}F_T\left(e^{\lambda_{232}t_i} - 1\right)}{\left[\begin{array}{c} 8\lambda_{238}\,^{238}F_T\,^{238}Ue^{\lambda_{238}t_i} + \frac{7}{137.818}\lambda_{235}\,^{235}F_T\,^{238}Ue^{\lambda_{235}t_i} + \\ 6\lambda_{232}\,^{232}F_T\,^{232}The^{\lambda_{232}t_i} + \lambda_{147}\,^{147}F_T\,^{147}Sme^{\lambda_{147}t_i} \end{array}\right]}$$

(a3)

$$\frac{\partial f}{\partial^{147}Sm} = -\frac{^{147}F_T\left(e^{\lambda_{147}t_i}-1\right)}{\left[\begin{array}{l}8\lambda_{238}{}^{238}F_T{}^{238}Ue^{\lambda_{238}t_i}+\dfrac{7}{137.818}\lambda_{235}{}^{235}F_T{}^{238}Ue^{\lambda_{235}t_i}+\\[2mm]6\lambda_{232}{}^{232}F_T{}^{232}The^{\lambda_{232}t_i}+\lambda_{147}{}^{147}F_T{}^{147}Sme^{\lambda_{147}t_i}\end{array}\right]}$$

460 (a4)

$$\frac{\partial f}{\partial^{238}F_T} = -\frac{8^{238}U\left(e^{\lambda_{238}t_i}-1\right)}{\left[\begin{array}{l}8\lambda_{238}{}^{238}F_T{}^{238}Ue^{\lambda_{238}t_i}+\dfrac{7}{137.818}\lambda_{235}{}^{235}F_T{}^{238}Ue^{\lambda_{235}t_i}+\\[2mm]6\lambda_{232}{}^{232}F_T{}^{232}The^{\lambda_{232}t_i}+\lambda_{147}{}^{147}F_T{}^{147}Sme^{\lambda_{147}t_i}\end{array}\right]}$$

(a5)

$$\frac{\partial f}{\partial^{235}F_T} = -\frac{7^{235}U\left(e^{\lambda_{235}t_i}-1\right)}{\left[\begin{array}{l}8\lambda_{238}{}^{238}F_T{}^{238}Ue^{\lambda_{238}t_i}+\dfrac{7}{137.818}\lambda_{235}{}^{235}F_T{}^{238}Ue^{\lambda_{235}t_i}+\\[2mm]6\lambda_{232}{}^{232}F_T{}^{232}The^{\lambda_{232}t_i}+\lambda_{147}{}^{147}F_T{}^{147}Sme^{\lambda_{147}t_i}\end{array}\right]}$$

(a6)

465

$$\frac{\partial f}{\partial^{232}F_T} = -\frac{6^{232}Th\left(e^{\lambda_{232}t_i}-1\right)}{\left[\begin{array}{l}8\lambda_{238}{}^{238}F_T{}^{238}Ue^{\lambda_{238}t_i}+\dfrac{7}{137.818}\lambda_{235}{}^{235}F_T{}^{238}Ue^{\lambda_{235}t_i}+\\[2mm]6\lambda_{232}{}^{232}F_T{}^{232}The^{\lambda_{232}t_i}+\lambda_{147}{}^{147}F_T{}^{147}Sme^{\lambda_{147}t_i}\end{array}\right]}$$

(a7)

$$\frac{\partial f}{\partial^{147}F_T} = -\frac{^{147}Sm\left(e^{\lambda_{147}t_i}-1\right)}{\left[\begin{array}{l}8\lambda_{238}{}^{238}F_T{}^{238}Ue^{\lambda_{238}t_i}+\dfrac{7}{137.818}\lambda_{235}{}^{235}F_T{}^{238}Ue^{\lambda_{235}t_i}+\\[2mm]6\lambda_{232}{}^{232}F_T{}^{232}The^{\lambda_{232}t_i}+\lambda_{147}{}^{147}F_T{}^{147}Sme^{\lambda_{147}t_i}\end{array}\right]}$$

(a8)

If ^{235}U was directly quantified, the derivatives for ^{238}U and ^{235}U are

470

$$\frac{\partial f}{\partial^{238}U} = -\frac{8^{238}F_T\left(e^{\lambda_{238}t_i}-1\right)}{\left[\begin{array}{l}8\lambda_{238}{}^{238}F_T{}^{238}Ue^{\lambda_{238}t_i}+7\lambda_{235}{}^{235}F_T{}^{235}Ue^{\lambda_{235}t_i}+\\[2mm]6\lambda_{232}{}^{232}F_T{}^{232}The^{\lambda_{232}t_i}+\lambda_{147}{}^{147}F_T{}^{147}Sme^{\lambda_{147}t_i}\end{array}\right]}$$

(a9)

$$\frac{\partial f}{\partial^{235}U} = -\frac{7^{235}F_T\left(e^{\lambda_{235}t_i}-1\right)}{\left[\begin{array}{l}8\lambda_{238}{}^{238}F_T{}^{238}Ue^{\lambda_{238}t_i}+7\lambda_{235}{}^{235}F_T{}^{235}Ue^{\lambda_{235}t_i}+\\[2mm]6\lambda_{232}{}^{232}F_T{}^{232}The^{\lambda_{232}t_i}+\lambda_{147}{}^{147}F_T{}^{147}Sme^{\lambda_{147}t_i}\end{array}\right]}$$

(a10)

and the denominator of the other components also change accordingly. Finally, with ^{235}U quantified directly, the overall
uncertainty propagation equation becomes:

$$\sigma_t = \sqrt{ \begin{aligned} & \left(\frac{\partial t}{\partial\, ^4He}\sigma_{He}\right)^2 + \left(\frac{\partial t}{\partial\, ^{238}U}\sigma_{238}\right)^2 + \left(\frac{\partial t}{\partial\, ^{235}U}\sigma_{235}\right)^2 + \left(\frac{\partial t}{\partial\, ^{232}Th}\sigma_{232}\right)^2 + \left(\frac{\partial t}{\partial\, ^{147}Sm}\sigma_{147}\right)^2 + \\[4pt] & 2\frac{\partial t}{\partial\, ^{238}U}\frac{\partial t}{\partial\, ^{235}U}\sigma_{238-235}{}^2 + 2\frac{\partial t}{\partial\, ^{238}U}\frac{\partial t}{\partial\, ^{232}Th}\sigma_{238-232}{}^2 + 2\frac{\partial t}{\partial\, ^{238}U}\frac{\partial t}{\partial\, ^{147}Sm}\sigma_{238-147}{}^2 + \\[4pt] & 2\frac{\partial t}{\partial\, ^{235}U}\frac{\partial t}{\partial\, ^{232}Th}\sigma_{235-232}{}^2 + 2\frac{\partial t}{\partial\, ^{235}U}\frac{\partial t}{\partial\, ^{147}Sm}\sigma_{235-147}{}^2 + 2\frac{\partial t}{\partial\, ^{235}Th}\frac{\partial t}{\partial\, ^{147}Sm}\sigma_{232-147}{}^2 + \\[4pt] & \left(\frac{\partial t}{\partial\, ^{238}F_T}\sigma_{Ft238}\right)^2 + \left(\frac{\partial t}{\partial\, ^{235}F_T}\sigma_{Ft235}\right)^2 + \left(\frac{\partial t}{\partial\, ^{232}F_T}\sigma_{Ft232}\right)^2 + \left(\frac{\partial t}{\partial\, ^{147}F_T}\sigma_{Ft147}\right)^2 + \\[4pt] & 2\frac{\partial t}{\partial\, ^{238}F_T}\frac{\partial t}{\partial\, ^{235}F_T}\sigma_{Ft238-Ft235}{}^2 + 2\frac{\partial t}{\partial\, ^{238}F_T}\frac{\partial t}{\partial\, ^{232}F_T}\sigma_{Ft238-Ft232}{}^2 + \\[4pt] & 2\frac{\partial t}{\partial\, ^{238}F_T}\frac{\partial t}{\partial\, ^{147}F_T}\sigma_{Ft238-Ft147}{}^2 + 2\frac{\partial t}{\partial\, ^{235}F_T}\frac{\partial t}{\partial\, ^{232}F_T}\sigma_{Ft235-Ft232}{}^2 + \\[4pt] & 2\frac{\partial t}{\partial\, ^{235}F_T}\frac{\partial t}{\partial\, ^{147}F_T}\sigma_{Ft235-Ft147}{}^2 + 2\frac{\partial t}{\partial\, ^{232}F_T}\frac{\partial t}{\partial\, ^{147}F_T}\sigma_{Ft232-Ft147}{}^2 \end{aligned} }$$

(a11)

Appendix B: Implications of gaussian input uncertainties in HeCalc

Negative dates are permitted in the probability distributions produced by HeCalc; this is because the input
distributions are presumed to be gaussian, meaning that if the input variables have high relative errors, negative molar
amounts of U, Th, Sm, and He are possible. This behavior is formally correct for gaussian uncertainties, albeit non-physical.
For low count rates associated with high relative uncertainty, a Poisson distribution (rather than gaussian distribution) is
appropriate, and would prevent negative input values. However, high relative input uncertainties are generally due to a
measurement being near or below background rather than low count rates where the underlying poisson distribution of the
data is not well approximated by a gaussian. As a result, there are potential instances of negative molar amounts included in
the Monte Carlo calculations. In some rare instances when a negative amount of a given parent nuclide is produced in the
generation of random data, the (U-Th)/He date equation may have multiple or no solutions. In these cases, the result is
simply removed from the sample of calculated ages. The total number of such removals is tracked, and if the proportion
removed exceeds the requested precision level, all results associated with the Monte Carlo simulation is reported as NaN
(i.e., "not a number") and only the linear uncertainty propagation results are returned. For typical inputs of routine analyses
with a few percent relative uncertainty (Sect. 5), the impact of this phenomenon is negligible.

Appendix C: Uncertainty in date as a function of input uncertainties

We examined the overall behavior of date uncertainty from 0 to 4.6 Ga as a function of relative input uncertainties
of 1%, 5% and 20% on ^{4}He (Fig. C1a), radionuclides (Fig. C1b) and isotope-specific F_T values (Fig. C1c). This range of
dates was generated by fixing the ^{238}U and ^{232}Th values while varying ^{4}He values (no ^{147}Sm was included because of its
generally negligible influence on apatite and zircon results). Th/U ratios representative of a typical zircon (based on the Fish
Canyon Tuff zircon reference standard), a typical apatite (from a compilation of apatite data; Sect. 5), and the Durango
apatite reference standard (0.6, 1.25, and 16.1, respectively) were used. For all calculations, an isotope-specific F_T value of

0.7 was applied to all isotopes to permit comparisons between raw and F_T-corrected dates (while isotope-specific values will differ in real data, we simplify these to a single value here). We initially explored the influence of individual uncertainties on the date by varying the relative uncertainty of one input parameter (^{4}He, radionuclides, or F_T) while fixing all other uncertainties at 0 (Fig. C1). We then evaluated how combinations of input uncertainties can influence the date (Fig. C2), although this is more fully evaluated in practical terms using real data, as in Sect. 5. For these exercises, we use the results from Monte Carlo uncertainty propagation, as this technique is in theory fully accurate (see Appendix E for further discussion). We used a constant number of simulations set at 10^8 to provide precise estimates of skew and comparisons between the Monte Carlo and linear uncertainty propagation methods. This number of simulations corresponds to a minimum precision of the mean date of ~0.0002% (2 µg/g).

For individual input uncertainties, at young dates the input and output relative uncertainties are similar. If all uncertainty is in the ^{4}He value or correlated F_T values, the relative date uncertainty is equivalent to the input uncertainty at zero age (Fig. C1a&c). For uncertainty in the radionuclides, the relative date uncertainty at zero age is approximately 80% the magnitude of the relative input uncertainty (a 4:5 ratio). The exact scaling between input and output uncertainties is dependent on the Th/U ratio (Fig. C1b&c).
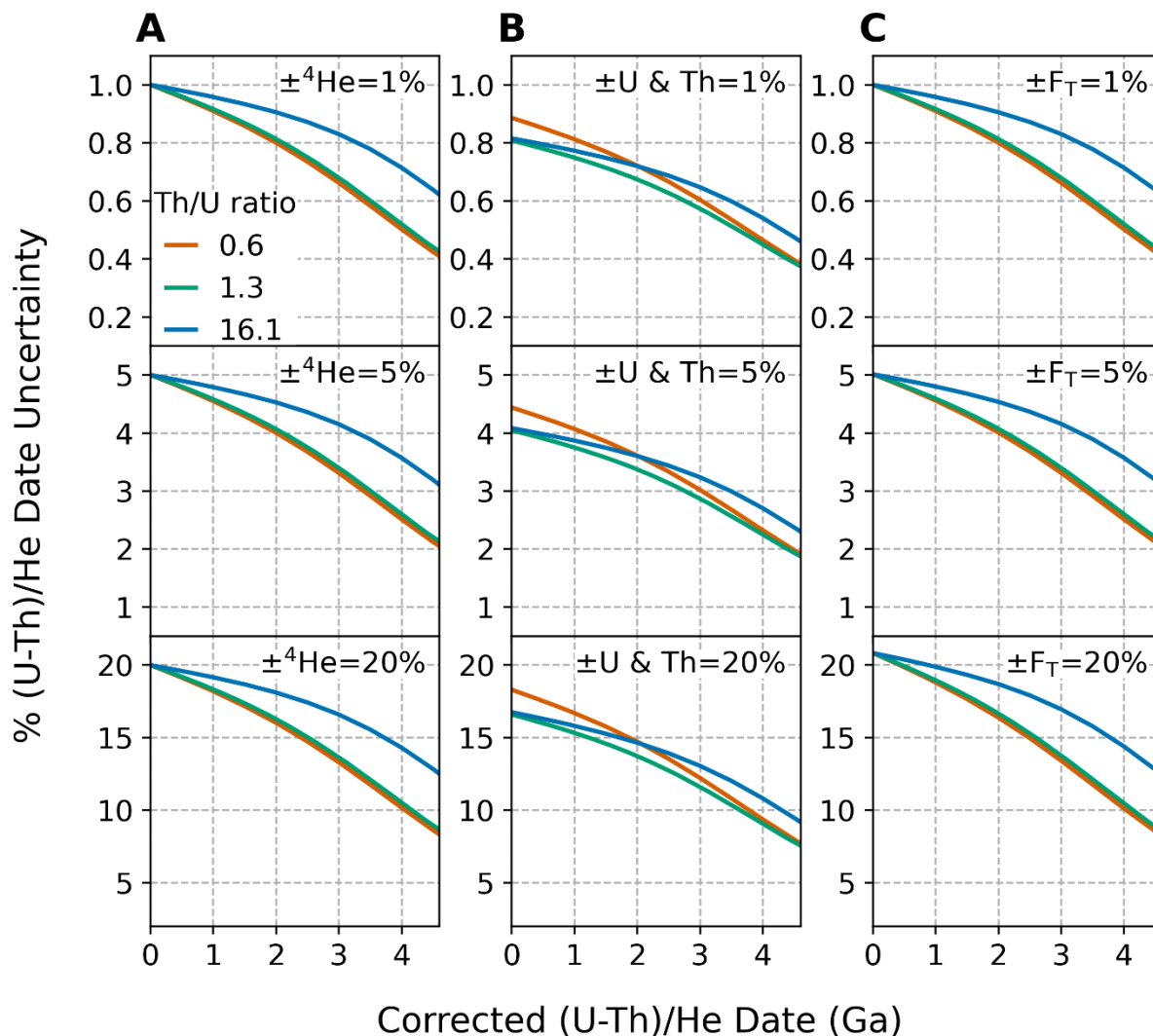
Figure C1: Corrected (U-Th)/He date uncertainties for dates of 0 to 4.6 Ga with input uncertainty on only one parameter and all others held at zero. Plots of percent relative uncertainty of the corrected date vs. corrected date for (a) uncertainty only in ^{4}He, (b) uncertainties only in radionuclides, and (c) uncertainties only in F_T, with fully correlated uncertainties ($r = 1$). Input uncertainties of 1% (top panels), 5% (middle panels), and 20% (bottom panels) are applied. The two 68% confidence intervals of the distributions resulting from Monte Carlo simulation were averaged to derive an equivalent 1σ uncertainty. The line colors correspond to the Th/U ratio for typical zircon (0.61, green curve, derived from the Fish Canyon Tuff zircon reference standard), for typical apatite (1.25 orange curve; derived from apatite data compilation), and for the Durango apatite reference standard (16.1, blue curve).

The relative date uncertainty decreases with increasing absolute date for constant relative input uncertainties. For example, while uncertainty in ^{4}He has a one-to-one relationship with date uncertainty at zero age, at 4.6 Ga the date uncertainty is approximately half that of the input ^{4}He uncertainty (Fig. C1a). The same phenomenon is observed for uncertainty in radionuclides and F_T (Fig. C1b&c). The relative extent of decreasing uncertainty as a function of increasing

525 date is dependent on Th/U ratio and is independent of the magnitude of input uncertainty (i.e., the three vertically stacked panels in Fig. C1a, 3b, and 3c are identical aside from the scale of their y-axes).

Decreasing uncertainty with increasing date is also observed for multiple input uncertainties. Figure C2 illustrates examples of combining uncertainties with differing magnitudes in quadrature. At zero age, the uncertainty on the date introduced by each input parameter combines roughly in quadrature to provide the uncertainty on the date. For example, at

530 zero age, a 5% uncertainty in all parameters (^{4}He, radionuclides, correlated F_T uncertainty), each of which alone introduces a date uncertainty of 5%, 4%, and 5%, respectively, together yields a date uncertainty of 8.1% ($\sqrt{0.05^2 + 0.04^2 + 0.05^2} \cong 0.081$; solid line, Fig. C2b). Alternatively, if input uncertainties have highly differing magnitudes, the larger uncertainty will dominate and the resulting combined uncertainty will be approximately equal to the larger uncertainty. As an example, a 10% and 1% uncertainty combined in quadrature will result a 10.05% uncertainty. This behavior suggests that reducing the

535 magnitude of the largest input uncertainty will be the most effective means of reducing overall date uncertainty.
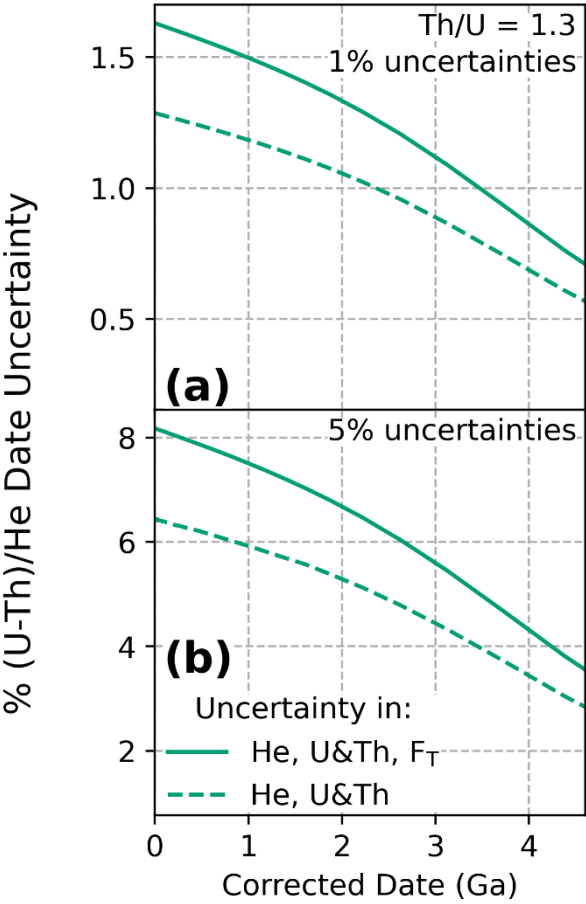
Figure C2: Corrected (U-Th)/He date uncertainties for dates of 0 to 4.6 Ga with uncertainty in multiple input parameters. Plots of percent realtive uncertainty in the corrected date vs. corrected date for the combination of (a) 1% uncertainty and (b) 5%

540 **uncertainty in ^{4}He and radionuclides, as well as in all input values. Calculations assume fully correlated uncertainty in isotope-specific F_T values ($r = 1$) for a Th/U ratio of 1.3 (derived from the Fish Canyon Tuff zircon reference standard).**

The phenomenon of decreasing uncertainty with increasing date is caused by the "roll over" of the helium ingrowth curve due to its nature as an exponential function. Because of this roll over, constant uncertainty in the independent variable

545 (i.e., [4]He or the radionuclides) will correspond to smaller uncertainty in the dependent variable (the date) as the value of the dependent variable increases. Fig. C3 is a schematic showing log plots of date vs. [4]He and date versus [238]U that illustrates this phenomenon. For young dates, the exponential term in the date equation (Eq. (2)) approaches zero, meaning that the relative uncertainties input to the He age equation will be roughly reflected in the output uncertainties (Sample 1, Fig. C3). For older dates, this exponential term becomes increasingly large, resulting in roll over of the ingrowth curve and reducing the date uncertainty relative to the inputs (Sample 2, Fig. C3). The exact form of this roll over is dictated by the relative

550 abundance of each radioisotope, resulting in the variations observed in Fig. C1 for differing Th/U values.
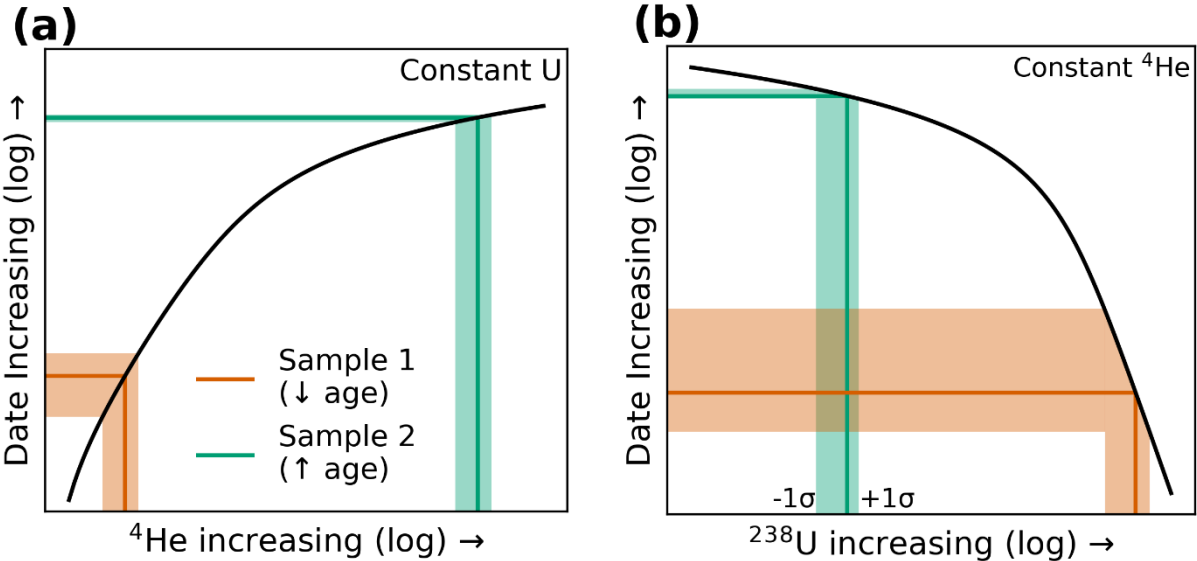
Figure C3: Schematics showing how non-linearity in the (U-Th)/He date equation causes decreasing uncertainty with increasing date. Black curves on log-log plots show (a) date increasing as a function of increasing [4]He with other parameters fixed, and (b) date decreasing as a function of increasing [238]U with other parameters fixed. Two example samples, one young (Sample 1, orange line)

555 **and one old (Sample 2, green line) are provided with gaussian constant percent relative uncertainty (1σ, depicted by the shaded region). The apparent asymmetry in the uncertainty along the x-axis is a result of the logarithmic plot. The non-linearity of the (U-Th)/He age equation is exaggerated for this schematic by decreasing the uranium decay constant to improve visibility of its effects. Note that in log-log space, the spread (i.e., uncertainty) in the x-axis is constant for constant input uncertainty, but the resulting uncertainty on the y-axis shrinks with increasing date.**

560 **Appendix D: Skew in distributions yielded by Monte Carlo uncertainty propagation**

Skew refers to the extent of asymmetry in the "tails" of a distribution (Fig. D1). For example, the skewed distribution in Fig. D1c is highly asymmetric, while the less skewed distribution in Fig. D1a is more symmetric. This asymmetry would most accurately be reported as separate positive and negative uncertainty values referring to the 68% confidence interval rather than the more typical 1σ uncertainty reporting of symmetric uncertainty (e.g., 100 [+11, -9] Ma

565 instead of 100 ±10 Ma). As discussed in section 5.2, we report skew in Monte Carlo-generated histograms by taking the percent difference between the positive and negative 68% confidence intervals with respect to the date, to generate a parameter that is more intuitive than unitless metric by which skew is typically defined.
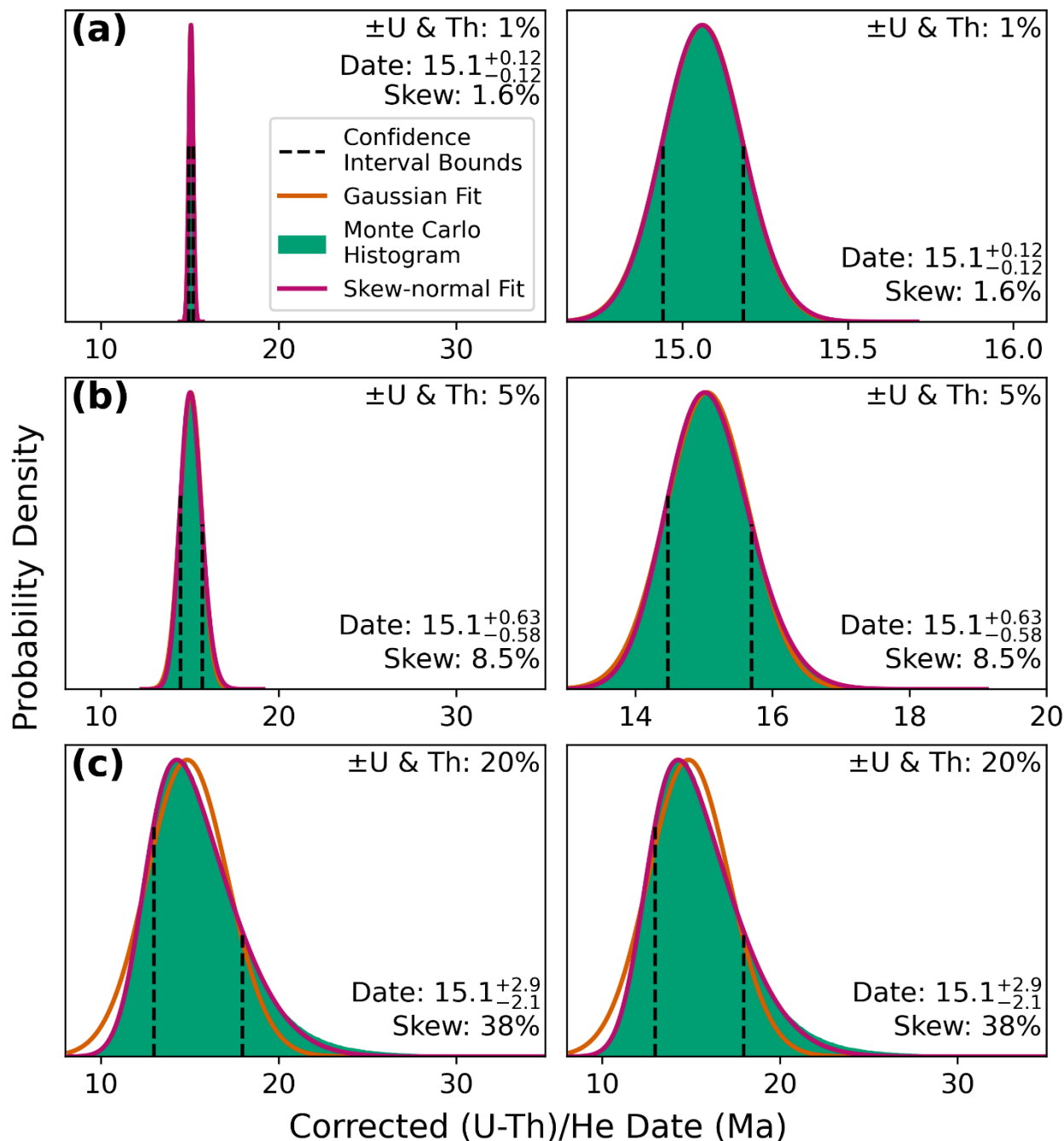
Figure D1: An illustration of how differing uncertainty affects the skew of date probability distributions for inputs yielding a date of 15.1 Ma (assuming a typical apatite Th/U ratio of 0.61). (a) Low radionuclide uncertainty of 1%, giving ~1.6% skew; (b) high radionuclide uncertainty of 5%, giving ~8.5% skew; and (c) extremely high radionuclide uncertainty of 20% (see discussion of real data in Sect. 5), giving ~38% skew. The gaussian fits in panels (a) and (b) are almost entirely concealed by the skew-normal fit plotted above it. The left column shows all distributions at the same scale, while the right-hand column zooms into the more precise (and less skewed) distributions to show detail.

575   The magnitude of skew correlates directly with the magnitude of input uncertainty (Fig. D1-D2). For low percent input uncertainties on all parameters, the magnitude of skew is low. For example, uncertainties of 1% for all inputs yield ≤2% skew for dates from 0 to 4.6 Ga (Fig. D2a-c, top panels). Only when the input uncertainties are larger does the effect of skew on the dates become substantial (Fig. D2a-c, middle and bottom panels). In the case of larger uncertainty in 4He (Fig. D2a, middle and bottom panels), skew increases from zero to progressively larger negative values at older dates. The inverse

580 is true for uncertainty in the radionuclides and F_T; skew is highest when uncertainty in these parameters is high for young dates and decreases with increasing age (Fig. D2b-c, middle and bottom panels). Note that although asymmetric uncertainties as high as ~40% can be yielded by radionuclide uncertainties of 20%, such large uncertainties are anomalous and do not typify most high-quality (U-Th)/He datasets (Sect. 5).
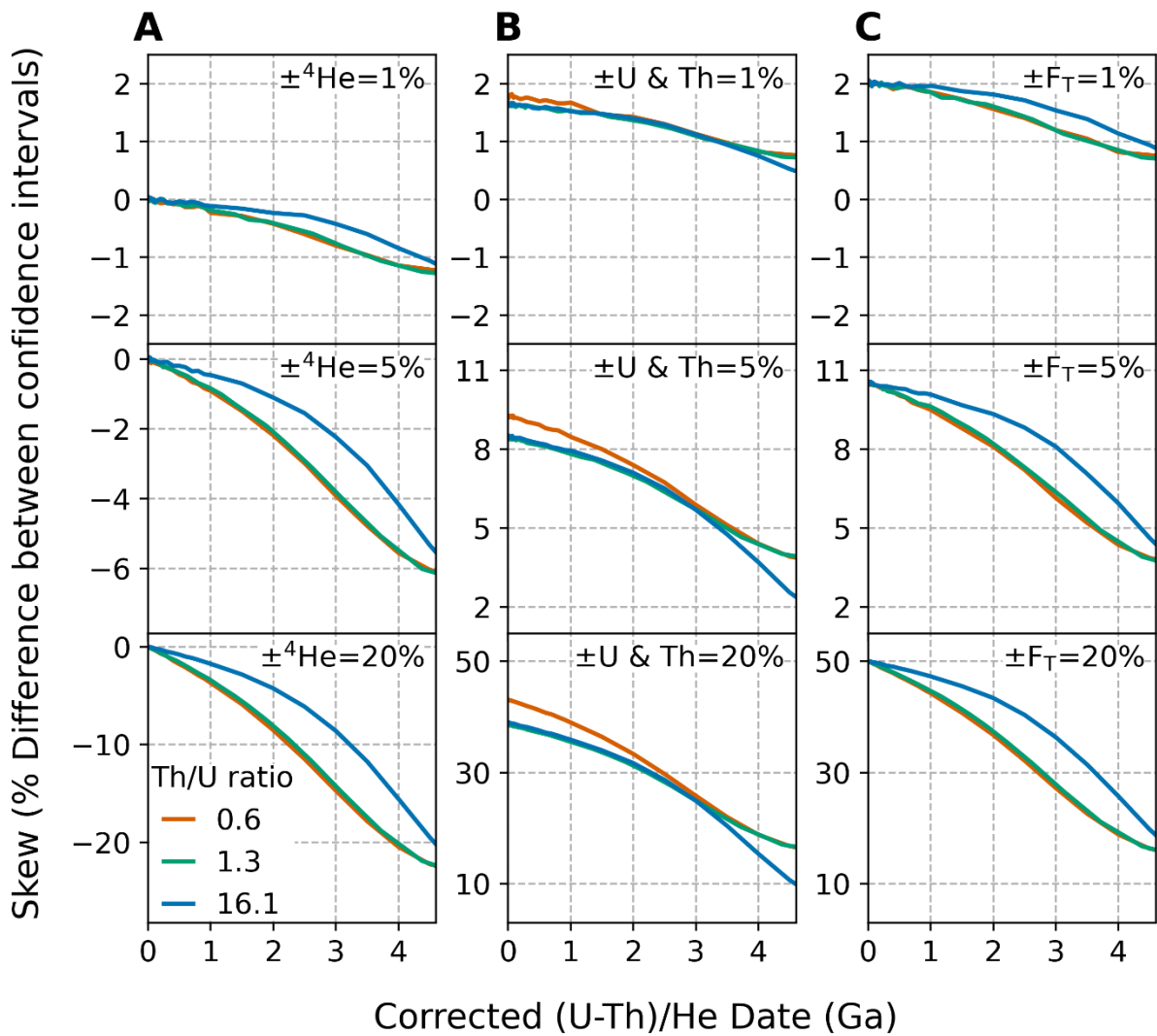
Figure D2: Illustration of the impact on skew from 0 to 4.6 Ga of varying input percent uncertainties while holding other uncertainties fixed at zero. Skew is shown as a percent difference between the 68% confidence intervals with respect to the nominal date value, as a function of input uncertainty for (a) ^{4}He, (b) radionuclides, and (c) F_T. Input uncertainties of 1% (top panels), 5% (middle panels), and 20% (bottom panels) were applied. The line colors correspond to the Th/U ratio for typical zircon (0.61, green

590 **curve, derived from the Fish Canyon Tuff zircon reference standard), for typical apatite (1.25 orange curve; derived from apatite data compilation), and for the Durango apatite reference standard (16.1, blue curve). Note that unlike Fig. C1, the y-axis scale is different for some panels.**

When uncertainty is included in multiple input parameters, the overall skew is a combination of the skew resulting from individual input uncertainties (Fig. D3). Unlike date uncertainty, which combines individual inputs in quadrature, the combination of skew from individual inputs does not follow an easily predictable trend. For input uncertainties of 1% and
595 5% for ^{4}He and the radionuclides only, the skew is largest at zero age (~1% and 5%, respectively), and declines with increasing age (dashed lines in Fig. D3). Because uncertainty in ^{4}He generates negative skew at older dates (Fig. D2a), the skew from these combined uncertainties becomes negative at dates $\gtrsim$3 Ga as the skew resulting from ^{4}He uncertainty overwhelms the skew from radionuclides, which has the opposite sign and is greatest at young dates (Fig. D2b). Similarly, for input uncertainties of 1% and 5% for all parameters (including F_T), the skew is largest at zero age (~2% and ~11%
600 respectively) and declines with decreasing age (to ~0% at 4.6 Ga; solid lines in Fig. D3).
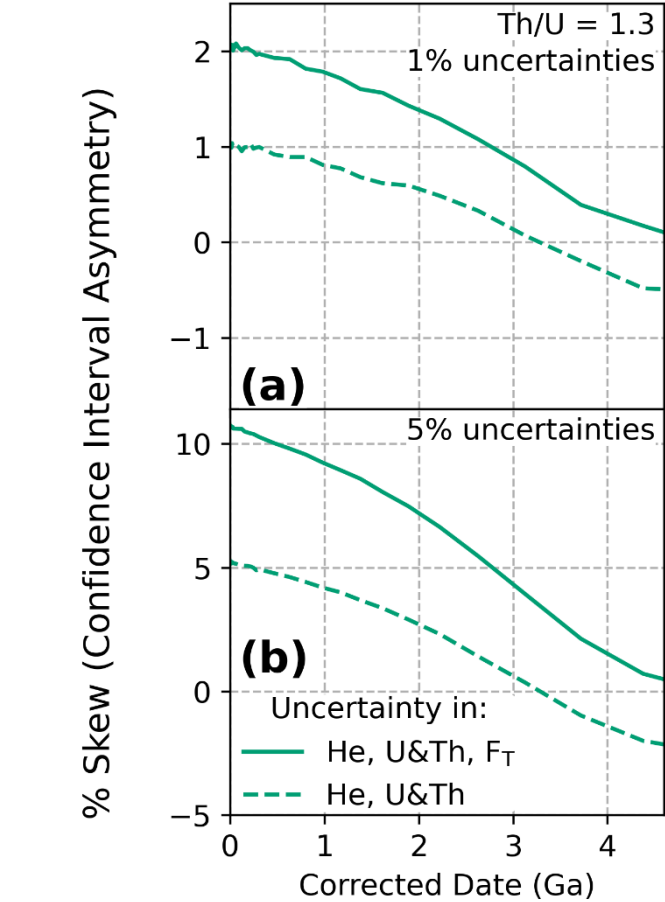
Figure D3: The skew in the date probability distribution resulting from combining multiple input uncertainties. Skew is shown as a percent difference between the 68% confidence intervals. This figure shows each possible combination of (a) 1% uncertainty and (b) 5% uncertainty in ^{4}He, radionuclides, and fully correlated F_T ($r = 1$) for a Th/U ratio of 1.3 (the green curve, derived from the
605 **Fish Canyon Tuff zircon reference standard).**

Appendix E: Comparison of linear and Monte Carlo uncertainty propagation results

        To compare linear and Monte Carlo error propagation derived uncertainties, we average the two 68% confidence intervals to determine uncertainty from both methods at the 1σ level. For data with high skew, this method provides a means

610   of comparing the scale of these two differing output distributions directly. The magnitude of the error in uncertainty estimation from linear uncertainty propagation due to nonlinearity in the date equation is proportional to the magnitude of the input uncertainties. As shown in Fig. E1a, for uncertainty in He alone, the Monte Carlo and linear methods yield identical results at younger dates, with linear uncertainty propagation beginning to underestimate the true uncertainty values at older dates as the absolute magnitude of ^{4}He uncertainty increases (reaching a maximum discrepancy of ~2% for input

615   uncertainties of 20% at 4.6 Ga). Uncertainty in radionuclides and F_T have the opposite effect; the discrepancy between the Monte Carlo and linear methods is greatest (~3% for input uncertainties of 20%, dependent on Th/U ratio and correlation in F_T uncertainties) at zero age and decreases with increasing date. This small extent of error indicates that Monte Carlo and linear methods are in general agreement.
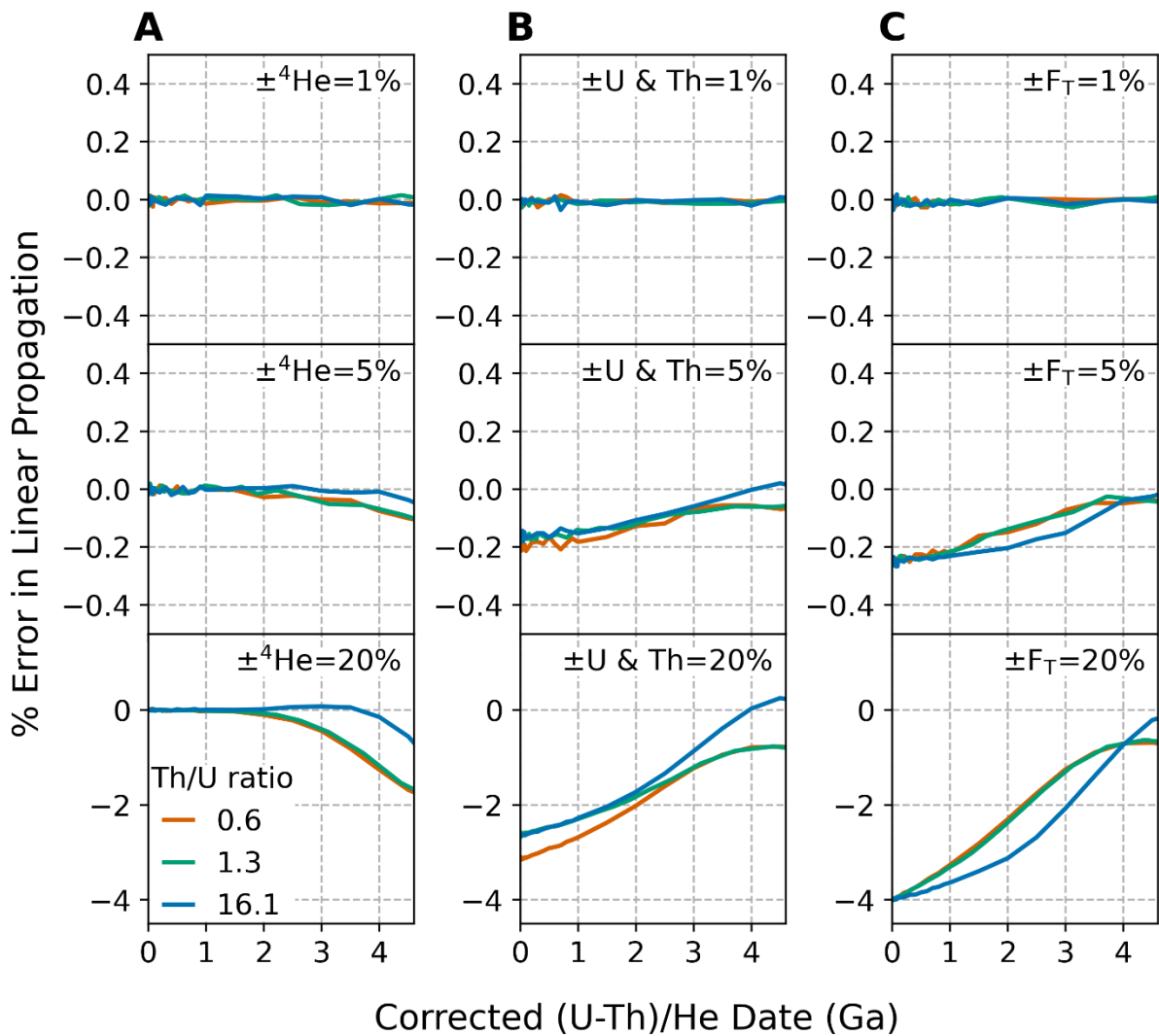
Figure E1: The percent error introduced by using linear uncertainty propagation instead of Monte Carlo uncertainty propagation for dates from 0 to 4.6 Ga. Error is shown for uncertainty in (a) ^{4}He, (b) radionuclides, and (c) F_T using the percent difference between the Monte Carlo and linear uncertainty propagation results, with the average 68% confidence intervals used to represent a single uncertainty value for the Monte Carlo results. Relative input uncertainties of 1% (top panels), 5% (middle panels), and 20% (bottom panels) were applied. The line colors correspond to the Th/U ratio for typical zircon (0.61, green curve, derived from the Fish Canyon Tuff zircon reference standard), for typical apatite (1.25 orange curve; derived from apatite data compilation), and for the Durango apatite reference standard (16.1, blue curve). Note that unlike Fig. C1, the y-axis scale is different for each panel.

As linear uncertainty propagation relies on an arithmetic calculation rather than random sampling, this method provides predictable and repeatable results for uncertainty calculations and is amenable to encoding in spreadsheet programs, facilitating the inclusion of the equations provided in Sect. 3.2 in existing spreadsheet-based workflows. However, the presence of skew in (U-Th)/He date uncertainties and the inaccuracies in uncertainty calculation induced by non-linearity in the (U-Th)/He age equation indicate that the more accurate Monte Carlo uncertainty propagation method is more universally applicable. Although in the past computational (in)efficiency was generally considered the weakness of Monte Carlo methods, running as many as one million Monte Carlo simulations in HeCalc takes less than one second on a modern computer for a typical sample. This number of random samples provides a sufficiently large population that output histograms are relatively smooth, yielding accurate uncertainty calculations with sufficient significant figures that the model-to-model variation induced by random sampling is negligible. As the Monte Carlo method in HeCalc is not excessively computationally intensive and provides both skew and accurate uncertainties, we suggest that the Monte Carlo method is preferable to linear uncertainty propagation in the (U-Th)/He system.

Code availability

Version 1.0.0 of the HeCalc software is available at 10.5281/zenodo.7315957. A windows executable application to run HeCalc is available through the latest release on the software's GitHub repository at https://github.com/Peter-E-Martin/HeCalc/releases/latest. Code documentation and installation instructions are also available on the GitHub repository.

Author contributions

PEM, RMF, and JRM conceptualized the project; JRM curated the data; PEM performed the formal analyses; RMF and JRM acquired funding; PEM, RMF, and JRM performed the investigation; PEM developed the methodology and wrote the software; RMF provided supervision; PEM wrote the original draft, and RMF and JRM reviewed and edited the manuscript.

Competing interests

The authors declare they have no competing interests.

Acknowledgements

We thank Noah McLean for numerous and very helpful discussions while developing HeCalc and writing this paper. HeCalc and this manuscript were greatly improved following discussions at the 17th International Conference on Thermochronology, in particular with Danny Stockli, Florian Hoffman, Marissa Tremblay and Kip Hodges. We appreciate helpful reviews by Pieter Vermeesch and Ryan Ickert that helped to clarify and streamline this manuscript. The (U-Th)/He analyses used in the data compilation presented here were generated by instrumentation funded by National Science Foundation award EAR-1126991 to Flowers, and awards EAR-1559306 and –1920648 to Flowers and Metcalf.

References

Anderson, G. M.: Error propagation by the Monte Carlo method in geochemical calculations, Geochimica et Cosmochimica Acta, 40, 1533–1538, https://doi.org/10.1016/0016-7037(76)90092-2, 1976.

Azzalini, A.: A Class of Distributions Which Includes the Normal Ones, Scandinavian Journal of Statistics, 12, 171–178, 1985.

Azzalini, A. and Capitanio, A.: Statistical applications of the multivariate skew normal distribution, Journal of the Royal Statistical Society: Series B (Statistical Methodology), 61, 579–602, https://doi.org/10.1111/1467-9868.00194, 1999.

Bevington, P. and Robinson, D. K.: Data Reduction and Error Analysis for the Physical Sciences, 3rd ed., McGraw-Hill Education, 344 pp., 2003.

Brown, R. W., Beucher, R., Roper, S., Persano, C., Stuart, F., and Fitzgerald, P.: Natural age dispersion arising from the analysis of broken crystals. Part I: Theoretical basis and implications for the apatite (U–Th)/He thermochronometer, Geochimica et Cosmochimica Acta, 122, 478–497, https://doi.org/10.1016/j.gca.2013.05.041, 2013.

Cooperdock, E. H. G., Ketcham, R. A., and Stockli, D. F.: Resolving the effects of 2-D versus 3-D grain measurements on apatite (U–Th) ⁄ He age data and reproducibility, Geochronology, 1, 17–41, https://doi.org/10.5194/gchron-1-17-2019, 2019.

Efron, B. and Tibshirani, R.: Bootstrap Methods for Standard Errors, Confidence Intervals, and Other Measures of Statistical Accuracy, Statistical Science, 1, 54–75, 1986.

Evans, N. J., McInnes, B. I. A., Squelch, A. P., Austin, P. J., McDonald, B. J., and Wu, Q.: Application of X-ray micro-computed tomography in (U–Th)/He thermochronology, Chemical Geology, 257, 101–113, https://doi.org/10.1016/j.chemgeo.2008.08.021, 2008.

Farley, K. A., Wolf, R. A., and Silver, L. T.: The effects of long alpha-stopping distances on (U□Th)/He ages, Geochimica et Cosmochimica Acta, 60, 4223–4229, https://doi.org/10.1016/S0016-7037(96)00193-7, 1996.

Fitzgerald, P. G., Baldwin, S. L., Webb, L. E., and O'Sullivan, P. B.: Interpretation of (U–Th)/He single grain ages from slowly cooled crustal terranes: A case study from the Transantarctic Mountains of southern Victoria Land, Chemical Geology, 225, 91–120, https://doi.org/10.1016/j.chemgeo.2005.09.001, 2006.

Flowers, R. M. and Kelley, S. A.: Interpreting data dispersion and "inverted" dates in apatite (U–Th)/He and fission-track datasets: An example from the US midcontinent, Geochimica et Cosmochimica Acta, 75, 5169–5186, https://doi.org/10.1016/j.gca.2011.06.016, 2011.

Flowers, R. M., Ketcham, R. A., Shuster, D. L., and Farley, K. A.: Apatite (U–Th)/He thermochronometry using a radiation damage accumulation and annealing model, Geochimica et Cosmochimica Acta, 73, 2347–2365, https://doi.org/10.1016/j.gca.2009.01.015, 2009.

Flowers, R. M., Zeitler, P. K., Danišík, M., Reiners, P. W., Gautheron, C., Ketcham, R. A., Metcalf, J. R., Stockli, D. F., Enkelmann, E., and Brown, R. W.: (U-Th)/He chronology: Part 1. Data, uncertainty, and reporting, GSA Bulletin, https://doi.org/10.1130/B36266.1, 2022.

Gallagher, K.: Transdimensional inverse thermal history modeling for quantitative thermochronology, Journal of Geophysical Research: Solid Earth, 117, https://doi.org/10.1029/2011JB008825, 2012.

Gautheron, C., Tassan-Got, L., Barbarand, J., and Pagel, M.: Effect of alpha-damage annealing on apatite (U–Th)/He thermochronology, Chemical Geology, 266, 157–170, https://doi.org/10.1016/j.chemgeo.2009.06.001, 2009.

695   Glotzbach, C., Lang, K. A., Avdievitch, N. N., and Ehlers, T. A.: Increasing the accuracy of (U-Th(-Sm))/He dating with 3D grain modelling, Chemical Geology, 506, 113–125, https://doi.org/10.1016/j.chemgeo.2018.12.032, 2019.

Guenthner, W. R., Reiners, P. W., Ketcham, R. A., Nasdala, L., and Giester, G.: Helium diffusion in natural zircon: Radiation damage, anisotropy, and the interpretation of zircon (U-Th)/He thermochronology, American Journal of Science, 313, 145–198, https://doi.org/10.2475/03.2013.01, 2013.

700   Herman, F., Braun, J., Senden, T. J., and Dunlap, W. J.: (U–Th)/He thermochronometry: Mapping 3D geometry using micro-X-ray tomography and solving the associated production–diffusion equation, Chemical Geology, 242, 126–136, https://doi.org/10.1016/j.chemgeo.2007.03.009, 2007.

Hiess, J., Condon, D. J., McLean, N., and Noble, S. R.: 238U/235U Systematics in Terrestrial Uranium-Bearing Minerals, Science, 335, 1610–1614, https://doi.org/10.1126/science.1215507, 2012.

705   Hourigan, J. K., Reiners, P. W., and Brandon, M. T.: U-Th zonation-dependent alpha-ejection in (U-Th)/He chronometry, Geochimica et Cosmochimica Acta, 69, 3349–3365, https://doi.org/10.1016/j.gca.2005.01.024, 2005.

House, M. A., Farley, K. A., and Stockli, D.: Helium chronometry of apatite and titanite using Nd-YAG laser heating, Earth and Planetary Science Letters, 183, 365–368, https://doi.org/10.1016/S0012-821X(00)00286-7, 2000.

Ketcham, R. A.: Forward and Inverse Modeling of Low-Temperature Thermochronometry Data, Reviews in Mineralogy and
710   Geochemistry, 58, 275–314, https://doi.org/10.2138/rmg.2005.58.11, 2005.

Ketcham, R. A., Gautheron, C., and Tassan-Got, L.: Accounting for long alpha-particle stopping distances in (U–Th–Sm)/He geochronology: Refinement of the baseline case, Geochimica et Cosmochimica Acta, 75, 7779–7791, https://doi.org/10.1016/j.gca.2011.10.011, 2011.

Ketcham, R. A., Tremblay, M., Abbey, A., Baughman, J., Cooperdock, E., Jepson, G., Murray, K., Odlum, M., Stanley, J.,
715   and Thurston, O.: Report from the 17th International Conference on Thermochronology, Earth and Space Science Open Archive, https://doi.org/10.1002/essoar.10511082.1, 2022.

Martin, P.: HeCalc, , https://doi.org/10.5281/zenodo.5672830, 2022.

McLean, N. M., Bowring, J. F., and Bowring, S. A.: An algorithm for U-Pb isotope dilution data reduction and uncertainty propagation, Geochemistry, Geophysics, Geosystems, 12, https://doi.org/10.1029/2010GC003478, 2011.

720   Meesters, A. G. C. A. and Dunai, T. J.: A noniterative solution of the (U-Th)/He age equation, Geochemistry, Geophysics, Geosystems, 6, https://doi.org/10.1029/2004GC000834, 2005.

Murray, K. E., Orme, D. A., and Reiners, P. W.: Effects of U–Th-rich grain boundary phases on apatite helium ages, Chemical Geology, 390, 135–151, https://doi.org/10.1016/j.chemgeo.2014.09.023, 2014.

O'Hagan, A. and Leonard, T.: Bayes estimation subject to uncertainty about parameter constraints, Biometrika, 63, 201–203,
725   https://doi.org/10.1093/biomet/63.1.201, 1976.

Peak, B. A., Flowers, R. M., Macdonald, F. A., and Cottle, J. M.: Zircon (U-Th)/He thermochronology reveals pre-Great Unconformity paleotopography in the Grand Canyon region, USA, Geology, 49, 1462–1466, https://doi.org/10.1130/G49116.1, 2021.

Possolo, A. and Iyer, H. K.: Invited Article: Concepts and tools for the evaluation of measurement uncertainty, Review of Scientific Instruments, 88, 011301, https://doi.org/10.1063/1.4974274, 2017.

Sturrock, C. P., Flowers, R. M., and Macdonald, F. A.: The Late Great Unconformity of the Central Canadian Shield, Geochemistry, Geophysics, Geosystems, 22, e2020GC009567, https://doi.org/10.1029/2020GC009567, 2021.

Wernicke, R. S. and Lippolt, H. J.: Dating of vein Specularite using internal (U+Th)/4He isochrons, Geophysical Research Letters, 21, 345–347, https://doi.org/10.1029/94GL00014, 1994.

Wolf, R. A., Farley, K. A., and Silver, L. T.: Helium diffusion and low-temperature thermochronometry of apatite, Geochimica et Cosmochimica Acta, 60, 4231–4240, https://doi.org/10.1016/S0016-7037(96)00192-5, 1996.

Wübbeler, G., Harris, P. M., Cox, M. G., and Elster, C.: A two-stage procedure for determining the number of trials in the application of a Monte Carlo method for uncertainty evaluation, Metrologia, 47, 317–324, https://doi.org/10.1088/0026-1394/47/3/023, 2010.

Zeigler, S. D., Metcalf, J. R., and Flowers, R. M.: A practical method for assigning uncertainty and improving the accuracy of alpha-ejection corrections and eU concentrations in apatite (U-Th)/He chronology, EGUsphere, 1–42, https://doi.org/10.5194/egusphere-2022-1005, 2022.

Zeitler, P. K., Herczeg, A. L., McDougall, I., and Honda, M.: U-Th-He dating of apatite: A potential thermochronometer, Geochimica et Cosmochimica Acta, 51, 2865–2868, https://doi.org/10.1016/0016-7037(87)90164-5, 1987.

Zeitler, P. K., Enkelmann, E., Thomas, J. B., Watson, E. B., Ancuta, L. D., and Idleman, B. D.: Solubility and trapping of helium in apatite, Geochimica et Cosmochimica Acta, 209, 1–8, https://doi.org/10.1016/j.gca.2017.03.041, 2017.